ALMA MATER STUDIORUM

Università di Bologna

SCHOOL OF ENGINEERING
- FORLÌ CAMPUS -

Second Cycle Master's Degree in
Aerospace Engineering
(LM-20)

MASTER'S THESIS
IN
Aerospace Structures

Cure Induced Residual Stresses on Thick Composite Components Manufactured by Additive Process

Candidate:
Onur Kıray

Supervisor:
Dr. Enrico Troiani

Co-supervisor:
Dr. Giacomo Struzziero
Dr. Julie Teuwen

Academic Year 2021-2022

Abstract

This study investigates the effect of an additive process in manufacturing of thick composites. Airstone 780 E epoxy resin and 785H Hardener system is used in the analysis since it is widely used wind turbine blade, namely thick components. As a fiber, fabric by SAERTEX (812 g/m2) with a 0-90 degrees layup direction is used. Temperature overshoot is a major issue during the manufacturing of thick composites. A high temperature overshoot leads to an increase in residual stresses. These residual stresses are causing warping, delamination, dimensional instability, and undesired distortion of composite structures. A coupled thermo-mechanical model capable of predicting cure induced residual stresses have been built using the commercial FE software Abaqus®. The possibility of building thick composite components by means of adding a finite number of sub-laminates has been investigated. The results have been compared against components manufactured following a standard route. The influence of pre-curing of the sub-laminates has also been addressed and results compared with standard practice. As a result of the study, it is found that introducing additive process can prevent temperature overshoot to occur and benefits the residual stresses generation during the curing process. However, the process time required increases by 50% therefore increasing the manufacturing costs. An optimized cure cycle is required to minimize process time and cure induced defects simultaneously.

Acknowledgments

This MSc thesis is my final effort as a student in Aerospace Engineering at the University of Bologna. These two years were not trivial due to challenges at the university and being away from home for a long time. I am very grateful to Giacomo Struzziero, who has been supervising me for four months whenever I needed help. With his knowledge and guidance, I have found a way out in tough situations. My sincere thanks go to Dr. Julie Teuwen, who also supervised me at TU Delft and provided me helpful feedbacks. I also would like to thank Dr. Enrico Troiani, who gave me opportunity to study at TU Delft.

My deepest thanks go to my family for making many sacrifices for me to fulfill my dreams. Last but not least, I would like to thank my girlfriend, Sezin, for supporting me in these two years of adventure. You have been my will to endure everything in this journey.

Table of Contents

List of Figures

List of Tables

List of Acronyms

GFRP - Glass Fiber Reinforced Plastic

VARTM – Vacuum Assisted Resin Transfer Molding

MRCC – Manufacturer's Recommended Cure Cycle

RTM – Resin Transfer Molding

LCM – Liquid Composite Molding

CAE – Computer Aided Engineering

SDV – Solution Dependent Variables

1 Introduction

1.1 Project Motivation

Over the last decades, composite parts expanded their number of applications and started to replace conventional metal part. They are chosen over metals due to their lightweight, higher strength and stiffness and resistance to the corrosion and fatigue [1]. Commonly used composite structures are thin layer laminated structures which are generally range between 2mm to 20mm. In past decades, manufacturers enlarged their capability of manufacturing thicker components. However, thicker components provide additional complexity in term of manufacturing. Today it is possible to manufacture center wing box with composite materials even though thickness of the loading positions exceeds traditional thickness of composite materials [2]. One other industry that adopted manufacturing thick (i.e. 50 mm) and ultra-thick (i.e. 100mm) parts is wind industry. Wind turbine blades are one of the components which are manufactured by composite materials. Figure 1.1 shows the mold for the B75 blade. It is a blade 75 meters long manufactured with glass fiber reinforced plastic (GFRP). At the root section wall thickness reaches 100mm. Manufacturing these components in a single piece poses a significant challenge because of the low transverse thermal conductivity of composite materials. As thickness of component increases, more violent exothermic reaction develops generating a significant thermal gradient through thickness which consequently leads to residual stresses. The aim of this is study is to investigate the residual stresses generated during the cure phase and put forward a way to reduce these stresses by changing manufacturing process. Recently, it has been shown that partially cured components retain interfacial properties as long as gelation point has not been exceeded [3]. The finding has opened up the possibility to manufacture components layer by layer initiating the cure at a fraction of the total thickness. In this project

the concept of manufacturing thick composite parts by adding pre-cured sub-laminates is investigated. By doing so, the chemical potential of the resin will be exploited at a fraction of the total thickness therefore reduction in temperature overshoots compared to standard routes are expected. The additive process concept here developed is a variation of the Vacuum Assisted Resin Transfer Molding (VARTM).

1.2 Research objectives

The aim of this project is to investigate the effect of additive VARTM process on temperature overshoot and residual stresses generation in thick composites. The purpose of additive VARTM process is to reduce the temperature overshoot experienced during manufacturing of thick composites. Additionally, the influence of process parameters such as the level of pre-curing of sub-laminates, ramp rate, and convection coefficient is investigated. At the end of the study, cure cycle recommendations for the manufacturing which results in less residual stresses are provided. The following objectives formulated in the shape of research questions should be answered during the study to reach the aim of the project:

1) What is the effect of additive process on the thick composites?
    - What is the effect of additive VARTM process on the temperature overshoot?
    - What is the link between reduced temperature overshoot and the residual stresses?
    - What is the effect of using pre-cured sub-laminates in additive process?

2) How does the pre-cure level of sub-laminates affect the temperature overshoot and residual stresses?

3) How do cure cycle parameters reduce residual stresses while ensuring good part quality (i.e. minimum degree of cure over the whole part)?

1.3 Thesis outline

The first and the current chapter provides information about the motivation and the research questions of this project.

Chapter two includes literature research related to the composite manufacturing, curing process and additive process of the composite materials.

Chapter three gives information about how the model is created in ABAQUS and how does the subroutine work. There are three different types of models created in this study. The differences between them have been described and additionally some hints have been made.

Chapter four reports the results in three parts. The first part explains the results for one case which is manufactured by MRCC. The second part discusses the effect of different manufacturing methods and process variables. The last part is a study that shows the most effective way to deal with uncured regions.

Chapter five presents results obtained at the end of the study and suggests recommendations for future possible works.

2 Literature Research

2.1 Liquid Composite Molding Processes

Resin Transfer Molding (RTM) is a manufacturing method within liquid composite molding (LCM). Figure 2.1 describes the main manufacturing steps of RTM. The first step in RTM is manufacturing of preforms. Once preforms are ready, they are placed into one side of the mold and then matching mold closes and resin injection can initiate. Thermosetting resins are most used type of resins used during RTM application. Due to low viscosity of thermosetting resins, they provide better injection and prevents possible dry spots to occur [4]. Resin can be injected into single or multiple inlets by application of pressure. After impregnation of preforms are completed, cure phase starts and once cure cycle is completed, demolding finalizes the manufacturing process.

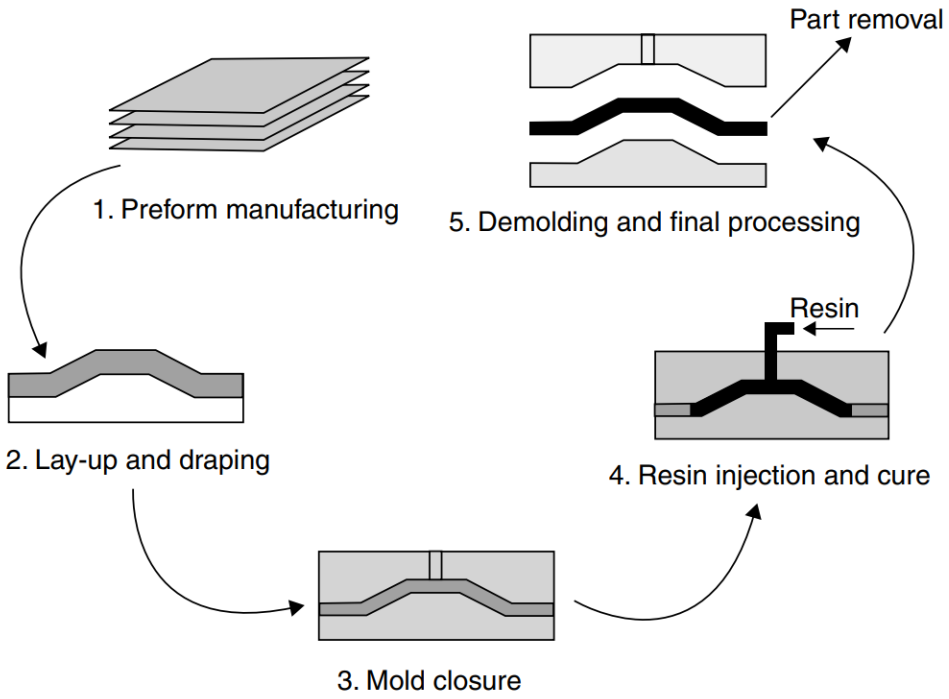

Figure 2.1: Scheme of RTM Process [5]

Vacuum Assisted Resin Transfer Molding (VARTM) is a liquid composite molding technique which is usually used to manufacture large scale structures [6]. It is a technique where dry fibers are infused by the resin with the application of vacuum pressure. Unlike Resin Transfer Molding (RTM) only a single mold is used, and resin drawn into the vacuum bag by vacuum instead of application of pressure. Dry fibers are placed on a mold surface within a plastic bag. In order to infuse the resin a vacuum system is used. creates voids. When the infusion stage is completed the cure stage begins.

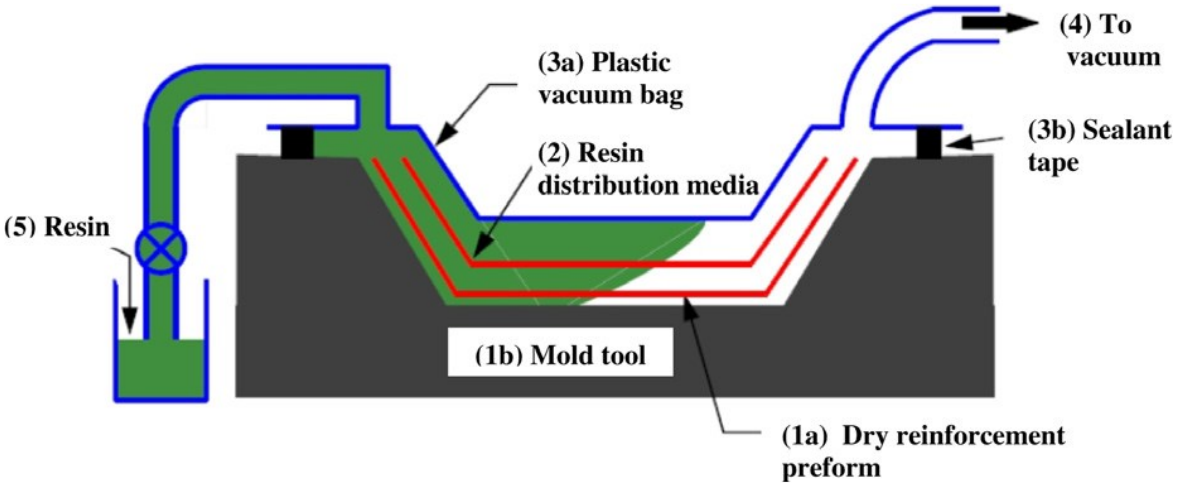

Figure 2.2 Scheme of VARTM Setup [7]

The advantages of VARTM can be mentioned as [8]:

- Higher fiber to resin ratio compared with the other manufacturing methods.
- Mold material selection and tooling method selection are more flexible.
- Large part manufacturing ability and better dimension accuracy.

On the other hand, the disadvantages can be mentioned as [8]:

- Limited injection speed which causes slower step.
- Lower quality of surface on the vacuum bagging side.
- Vacuum bag materials are not reusable so these materials should be prepared individually for the process.

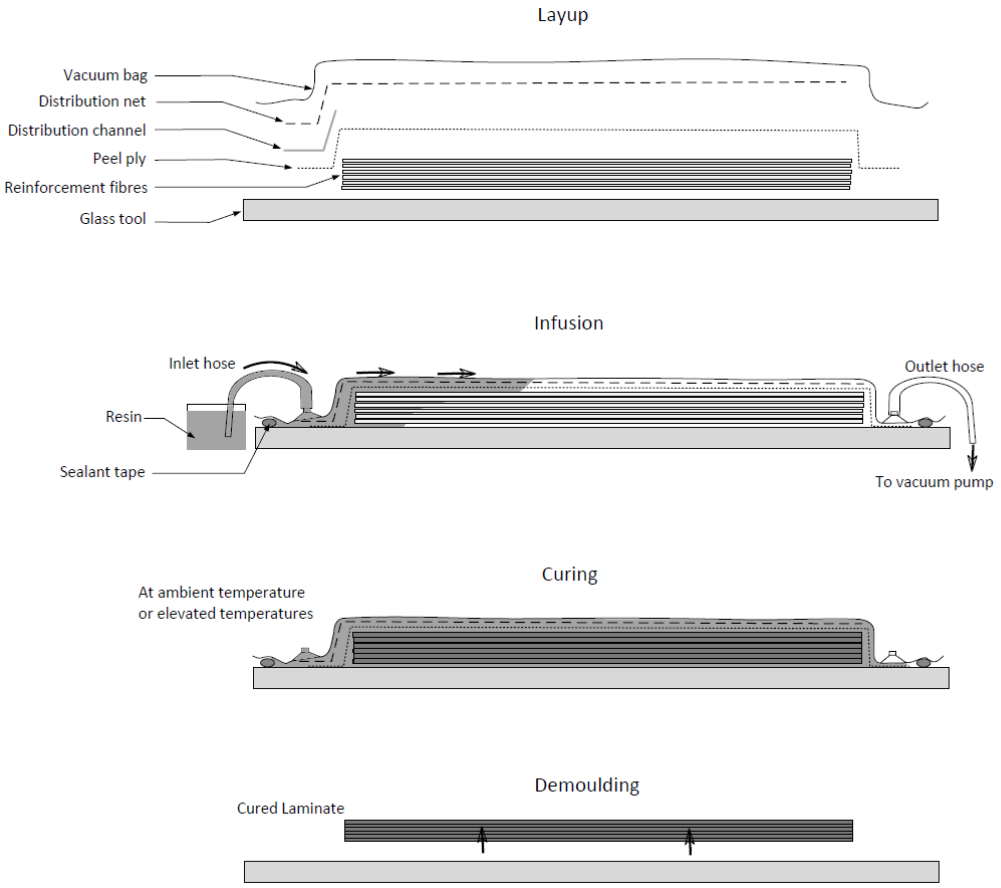

Figure 2.3: Scheme of VARTM Procedure [9]

Additive VARTM process is a variation of VARTM that is conceptualized in this study, which splits the manufacturing of thick components into lower thicknesses sub-laminates. The part that is going to be manufactured is divided into sub-laminates. Process starts with laying first set of dry fabrics, after infusion, impregnated fibers are pre-cured up to a prescribed degree of cure. Afterwards, dry fabrics are laid on top of the first pre-cured sub-laminate and a second infusion takes place. This procedure repeats until all the sub-laminates are fully cured and desired thickness is achieved. Figure 2.4 shows the manufacturing schematic of additive VARTM process. Pre-cured sub-laminates can also be manufactured in one single infusion and cure and then piled up together to finalize the cure; making the process a two-step process. The difference between VARTM and additive VARTM process is a multi-infusion and multi-curing process rather than single infusion and cure. In the figure, t and its

subscript show the time when sub-laminate is added and α shows the degree of cure of the sub-laminate that is being added to the structure.

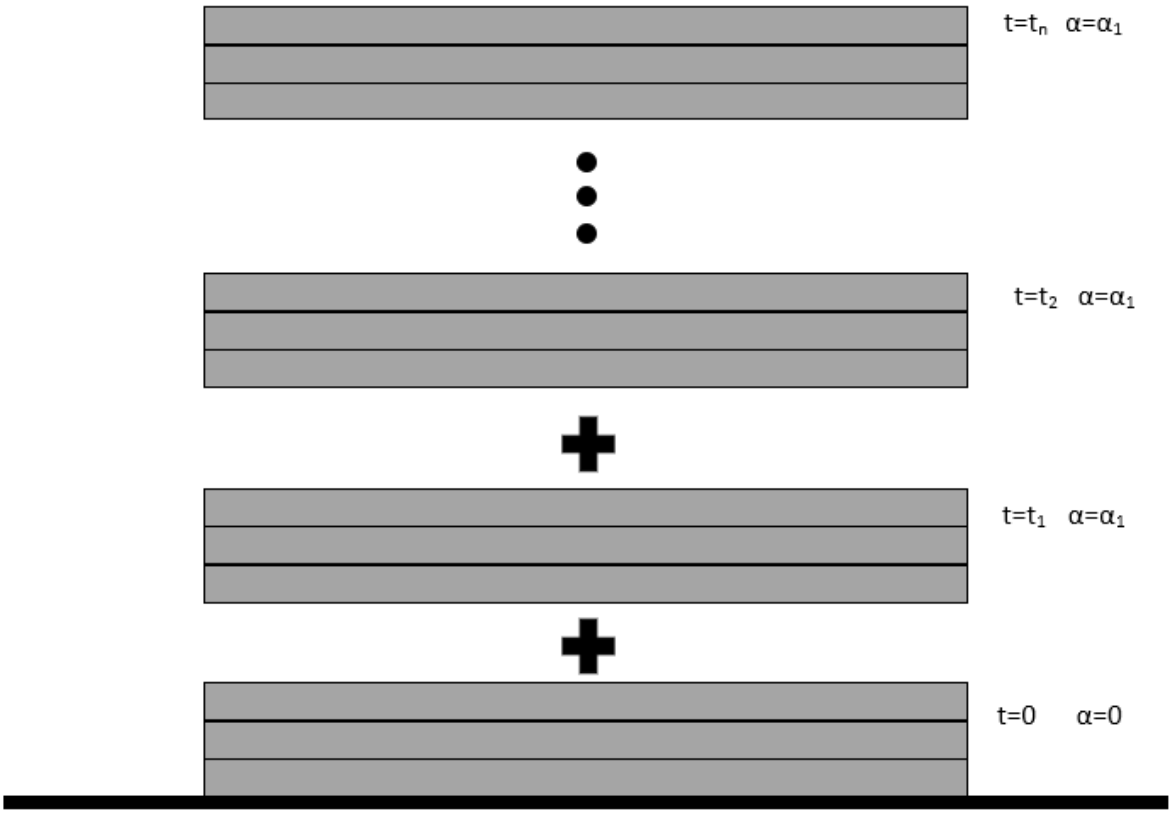

Figure 2.4: Scheme of additive VARTM process

2.2 Thermophysical properties

On the perspective of evolution of residual stresses, curing phase is the most important step. Once curing of the resin starts, the monomer molecules first undergo chain formation and linear growth through polymerization, then the resulting molecular chains form cross-links so that a large rigid three-dimensional molecular network is formed [10]. Figure 2.5 shows the different phases of curing and development of polymerization.

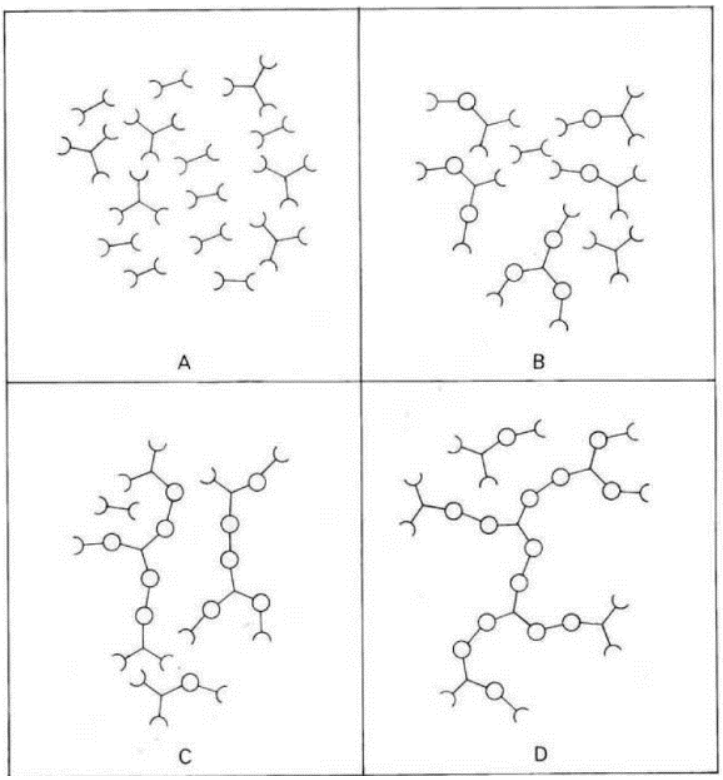

Figure 2.5: Curing process of a thermoset resin in different phases [11] a) monomers before cure phase b) beginning of the cure phase c) gelation stage: continuous but not complete network d) fully cured network

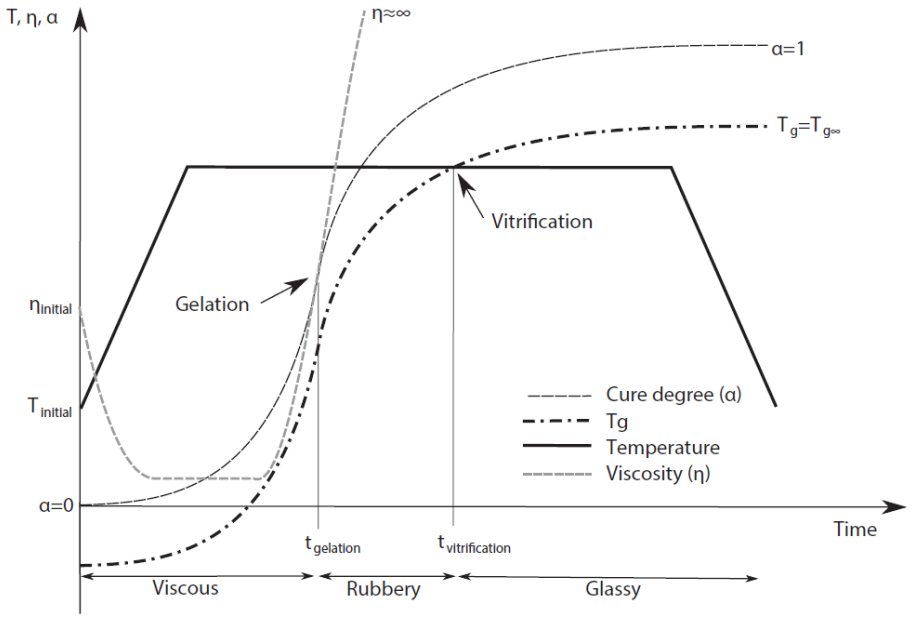

Figure 2.6 Schematic of evolution of cure degree, Tg and viscosity as time increases for a given cure cycle [9]

During the cure cycle three main states can be considered (see figure 2.6). (I) Viscous liquid state, (II) rubbery solid state after gelation and (III) Glassy solid state after vitrification. During these main three states, thermal and mechanical properties of the resin experiences dramatic changes [9].

The identification of the gel point is critical for thermoset processing since up to this point the polymer resin can still flow. At the gel point, a thermosetting resin will undergo a transition from a viscous liquid to viscoelastic solid [12]. As the curing process continues, the density of crosslinks will continue to increase. Vitrification is the point where glass transition temperature and temperature of the resin get equal [13].

2.3 Cure Kinetics

There are several studies done to determine the relation of chemical reactions between time, temperature, and degree of cure [14,15]. When examining the cure

kinetics empirical models are used and these models can be categorized as two main categories:

1) Phenomenological Models
2) Mechanistic Models

Phenomenological Models are simplified equations which are modelled without considering the details of how reactive species take place in the reaction. Mechanistic models, on the other hand, are modelled from the balances of reactive species involved in the process [14]. Although mechanistic models are better to predict cure kinetics, deriving such a models can be complex and not be possible always. Although more than one reaction happens at the same time during the curing process, nth order rate equations are used to introduce reaction rate. The simplest equation can be expressed as [15]:

$$\frac{d\alpha}{dt} = K_i(1-\alpha)^n \qquad (2.1)$$

where n is the order of the equation, α is the degree of cure and, K_i is defined as Arrhenius-dependent rate constant.

$$K_i = A_i e^{\frac{-\Delta E_i}{RT}} \qquad (2.2)$$

where A_i is pre-exponential factor, R is the universal gas constant, T is the temperature and E_i is the activation energy of the i^{th} order [16]. In equation 2.1, there is no autocatalytic phenomenon added to the reaction rate constant K_i. For these types of model reaction start from a peak value then it decreases as degree of cure increases [16]. Some other reactions can be described starting from the zero or a value close to zero at the room temperature. These reactions are called autocatalytic reaction or n^{th} order + autocatalytic reaction [16]. Autocatalytic reaction can be described as [62,63]:

$$\frac{d\alpha}{dt} = K_i\alpha^m(1-\alpha)^n \qquad (2.3)$$

where K_i is an Arrhenius-dependent rate constant and m and n are reaction orders and α is the degree of cure. A summary of models for epoxy-based cure kinetics can be examined in Table 2.1.

	Model	Equation
1.	n^{th} order	$\frac{d\alpha}{dt} = K_i(1-\alpha)^n$
2.	Autocatalytic	$\frac{d\alpha}{dt} = K_i\alpha^m(1-\alpha)^n$
3.	n^{th} order + Autocatalytic	$\frac{d\alpha}{dt} = (K_1 + K_2\alpha^m)(1-\alpha)^n$
4.	Arrhenius-dependent rate constant	$K_i = A_i e^{\frac{-\Delta E_i}{RT}}$

Table 2.1 Cure kinetic models for epoxy resin systems [16]

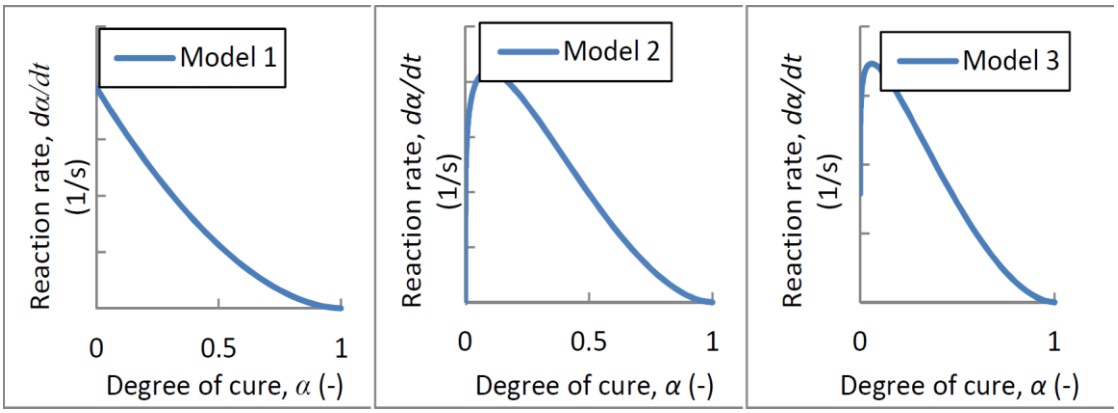

Figure 2.7 Reaction rate of different models for epoxy resins [16]

Figure 2.6 describes the reaction rate for different models as degree of cure increases. Model 3 is known as the Kamal-Sourour equation [17].

2.4 Cure induced residual stresses

Curing is a chemical process that creates cross linking polymer chains which result in toughening or hardening of material. For a composite material designing a cure cycle is important and not a trivial task. In case of badly designed cure cycles, additional stresses which are not desired may arise. These stresses arise due to several phenomenon like inherent anisotropy, chemical shrinkage, thermal expansion, and materials degradation or relaxation [18-23]. The scenario worsens in the case of manufacturing of thick components, since temperature overshoot and residual stresses can be significant [24-27]. Residual stresses developed have a significant effect on the mechanical properties of the final product [28-33]. To minimize residual stresses generation researchers have been working on optimization methodology able to identify optimal cure cycles to keep residual stresses generation to a minimum [34-39]. Often temperature overshoot has been used as objective to be minimized due to its link with residual stresses generation [64,83]. The Pareto fronts obtained showed that for a given thickness there are portions of the objective space inaccessible, meaning that given a certain thickness there will be a limit in the minimum achievable temperature overshoots [64].

Mechanism of Cure Induced Residual Stresses

It can be considered that the gelation is a starting point for the development of residual stresses. Before gelation point, since modulus is not developed, resin is not able to bear any stress [40]. Once gelation occurs, the elastic modulus builds up and this leads to the development of cure induced residual stresses [41]. The effect of coefficient of thermal expansion (CTE) is twofold: at micro and macro level. At micro level, the difference between CTE of resin and the fibers are too high to neglect. For a glass fiber, its CTE can be considered as positive in longitudinal direction while for carbon fiber as negative in longitudinal direction, and in transverse direction positive. For resin, CTE is significantly higher positive value than CTE of fiber [42].

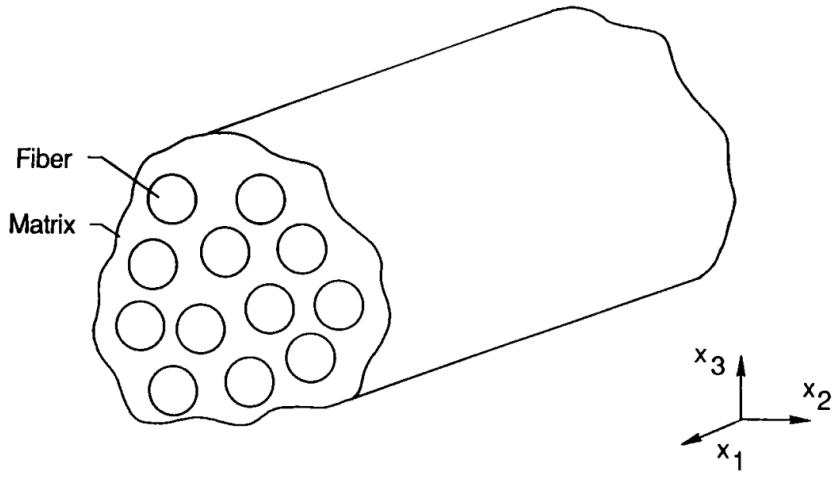

Figure 2.8 Fiber and Matrix geometry in micro level [43]

At macro level, there is a difference in ply-level expansion coefficients in the fiber and transverse directions, which leads in in-plane stresses in laminates [44-49]. These mechanism leads to a distortion in flat plat plates in case of not balanced and symmetric lay-ups [50-52]. After describing the role of CTE in cure induced residual stresses, secondly chemical shrinkage can be introduced. The chemical shrinkage happens due to the polymerization of the resin and depends linearly on degree of cure and it is non reversible [53-57]. Tool-part interaction is another source of residual stress development. It happens because of the CTE difference between manufactured part and tooling material [44]. The CTE of tool is usually higher than the composite material. This causes excessive elongation of tooling part compared to the composite material. As a result of this, shear stresses at the interface causes tension in the composite part. In case of forming gradient of stress in thickness direction, bending may occur [44,58-61].

2.5 Heat Transfer Modelling

The heat transfer equation for the curing problem can be represented as follows by ignoring the effect of resin flow during curing process [64]:

$$\rho_c c_{pc} \frac{\partial T}{\partial t} = \nabla(k_c \nabla T) + Q \qquad (2.4)$$

where ρ_c is the density, c_{pc} is the heat capacity, k is the thermal conductivity of the composite material, T is the temperature in Kelvin, t is the time and Q is the heat generated by the source [64]. Q can be described as :

$$Q = \rho_c v_r H_r \frac{d\alpha}{dt} \qquad (2.5)$$

where ρ_c is the density of the resin, v_r the resin volume fraction, H_r the total heat generated by the resin and $\frac{d\alpha}{dt}$ the reaction rate of the resin in 1/s [64]. For different type of resin systems, the curing mechanism is different because of the difference in molecules. For most of the epoxy resin systems, the n-th order cure kinetic model is used [63].

By combining the equations (2.4) and (2.5), the thermo-chemical energy balance equation can be written as:

$$\rho_c c_{pc} \frac{\partial T}{\partial t} = \nabla(k_c \nabla T) + \rho_c v_r H_r \frac{d\alpha}{dt} \quad (2.6)$$

To evaluate the evolution of the temperature through the composite thickness some researchers used 1-D heat transfer model [65] while other researchers solved the problem with 2-D and 3-D models [66, 67].

The prediction of residual stresses during the cure process can be addressed by solving a coupled thermo-mechanical problem. The strains can be identified as

mechanical, thermal, and chemical strains [68]. Section 3.2.4. describes mechanism of strains in a more detailed way. M, T and Sh superscripts defines the origin of strain which are mechanical, thermal, and chemical respectively while subscripts i,j=1, 2, 3 for orthogonal directions.

$$\varepsilon_{ij} = \varepsilon_{ij}^{M} + \varepsilon_{ij}^{T} + \varepsilon_{ij}^{Sh} \qquad (2.7)$$

$$\varepsilon_{ij}^{T} = \Delta T\{a_{ij}\} \qquad (2.8)$$

$$\varepsilon_{ij}^{Sh} = \Delta\alpha\left\{\gamma_{ij}\right\} \qquad (2.9)$$

where ΔT and $\Delta\alpha$ are change in temperature and degree of cure, respectively. $\{a_{ij}\}$ and $\left\{\gamma_{ij}\right\}$ is a vector notation that includes CTE and linear shrinkage coefficients. By combining equations 2.7,2.8 and 2.9, strain can be defined as:

$$\varepsilon_{ij} = [S]\sigma_{ij} + \Delta T\{a_{ij}\} + \Delta\alpha\left\{\gamma_{ij}\right\} \qquad (2.10)$$

Equation can be rewritten as following:

$$\sigma_{ij} = [C]\left[\varepsilon_{ij} - \left(\Delta T\{a_{ij}\} + \Delta\alpha\left\{\gamma_{ij}\right\}\right)\right] \qquad (2.11)$$

where [S] and [C] are compliance and stiffness matrix which is defined in section 3.2.5.

3 Methodology

The manufacturing methods used are VARTM by using MRCC and additive VARTM process. By using the additive VARTM process, on the other hand, manufacturing is done by applying more than one cure cycle either on pre-cured or uncured sub-laminates. The materials used in this study is non-crimp biaxial E-glass fibers fabric by SAERTEX (812 g/m^2) with a 0-90 degrees layup direction and Airstone 780E epoxy resin & Airstone 785H hardener system [85]. The density of the epoxy resin is 1150 kg/m^3 while 950 kg/m^3 for the hardener. The mix ratio of the epoxy resin and hardener is 100-31 by weight and 100-38 by volume. The volume fiber fraction of the system is set to 54%. The initial degree of cure is assumed to be 0.08 for uncured sub-laminates. The reason of this selection is to include degree of cure evolution of resin during injection since this resin system cures at the room temperature. Figure 3.1 shows cure cycles used in the study. The MRCC dictates ramp rate of 0.33 ^oC/min from 25^oC up to 70^oC and isothermal at 70^oC for four hours followed by cool down rate of 0.5^oC/min. The three other cure cycles shown which are used for Model 2, Model 3.1, and Model 3.2 with 0.32 pre-cure level. Model 2 has two intermediate cure cycles to cure sub-laminates up to 0.32 level of degree of cure that is followed by final step that has same cure cycle parameters with MRCC. For intermediate cure cycles dwell temperature is 45^oC and dwell duration is decided according to the desired degree of cure. For higher level of pre-cures than 0.32, dwell duration is increased and for lower values, it is decreased.

Model 3.1 has first step to pre-cure all sub-laminates up to 0.32 degree of cure afterwards all pre-cured sub-laminates are stacked together, and cure finalized by MRCC. Model 3.2 has two intermediate cure cycles to prepare pre-cured sub-laminates MRCC. Similar to Model 2, for Model 3.1 and Model 3.2 dwell temperature is 45 ^oC, the ramp rate 0.33^oC/min and the duration of dwell is decided by considering desired degree of cure for intermediate steps (i.e. 0.25, 0,32, 0.5 in this study).

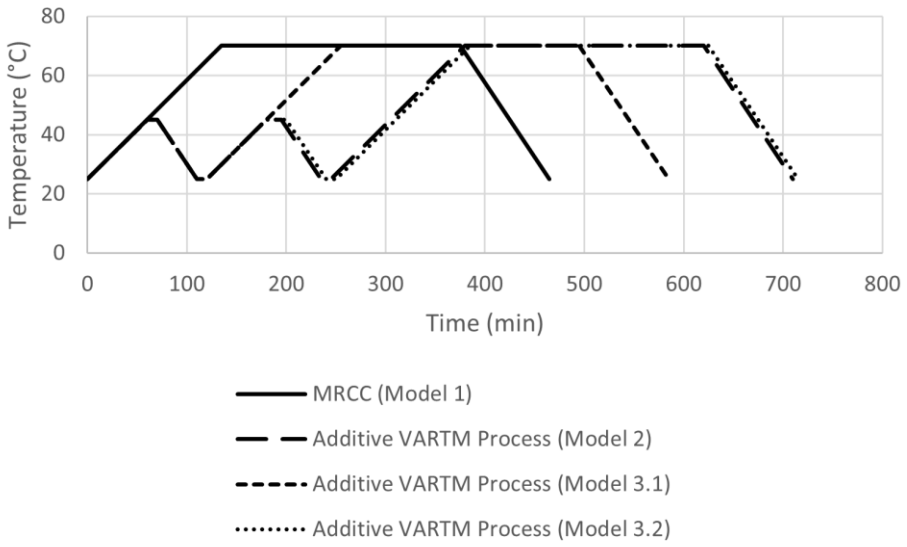

Figure 3.1: Cure Cycles Applied

The geometry represents a volumetric cube with 54 layers and 31.5 mm thickness at the center of the structures which are manufactured by using VARTM. A three dimensional 20-node brick element called "C3D20RT" is used for the solution coupled thermo-mechanical step. The total number of elements used is 2646. To simulate the mold heating applied in manufacturing for the resin to cure, a temperature boundary condition is applied at the bottom nodes following the cure cycle via the user subroutine DISP. At the top surface, natural convection is implemented by defining subroutine FILM with heat transfer coefficient of 8 W/m^2K and sink temperature of 25°C. Material properties describing the thermal and mechanical behavior of the composite material have been implemented by means of user subroutine UMAT. The properties are defined as function of temperature and degree of cure. The following subroutines are used:

SDVINI subroutine allows the user to assign initial value of solution-dependent state variables [69]. In this subroutine initial degree of cure and glass transition temperature is defined.

DISP subroutine allows the user to define the temperature at any desired node, surface or element [69]. In this model, it is used to set the temperature of the

bottom surface for desired cure cycle by specifying heating and cool down rate, dwell temperature and duration.

FILM subroutine allows the user to define sink temperature with a corresponding film coefficient [69]. In this model, it is used to simulate the natural convection during the curing process.

UMATH subroutine allows the user to define internal energy per mass and heat flux vector and their variation with respect to temperature [69]. These definitions must update the solution-dependent state variables. In this model, it is used to solve heat transfer problem through the thickness of the representative cube.

UMAT subroutine allows the user to define the mechanical constitutive behavior of a material [69]. It updates the stresses and solution-dependent state variables and must include material Jacobian matrix. In this model it is used to calculate the evolution of Tg, cure rate, degree of cure and their contribution to elastic, chemical and thermal strain which provides the evolution of stresses.

In the models, three different boundary conditions are used. The first one is a displacement/rotation type boundary conditions, the second one is temperature boundary condition which represents the cure cycle and third one is an interaction type boundary condition that simulates natural convection. To use minimum restriction on degree of freedom one of the corners at the bottom is pinned and neighboring corner in x-direction is restricted in y and z direction and neighboring corner in y-direction is restricted in z direction. This boundary condition allows bottom surface to expand in in-plane direction while restraining its movement in z-direction. For second boundary condition, the cure cycle temperature is directly implemented at the bottom nodes of the geometry. Third boundary condition that simulates natural convection is applied to the top nodes of the geometry. The representation of the boundary conditions can be seen below at Figure 3.2.

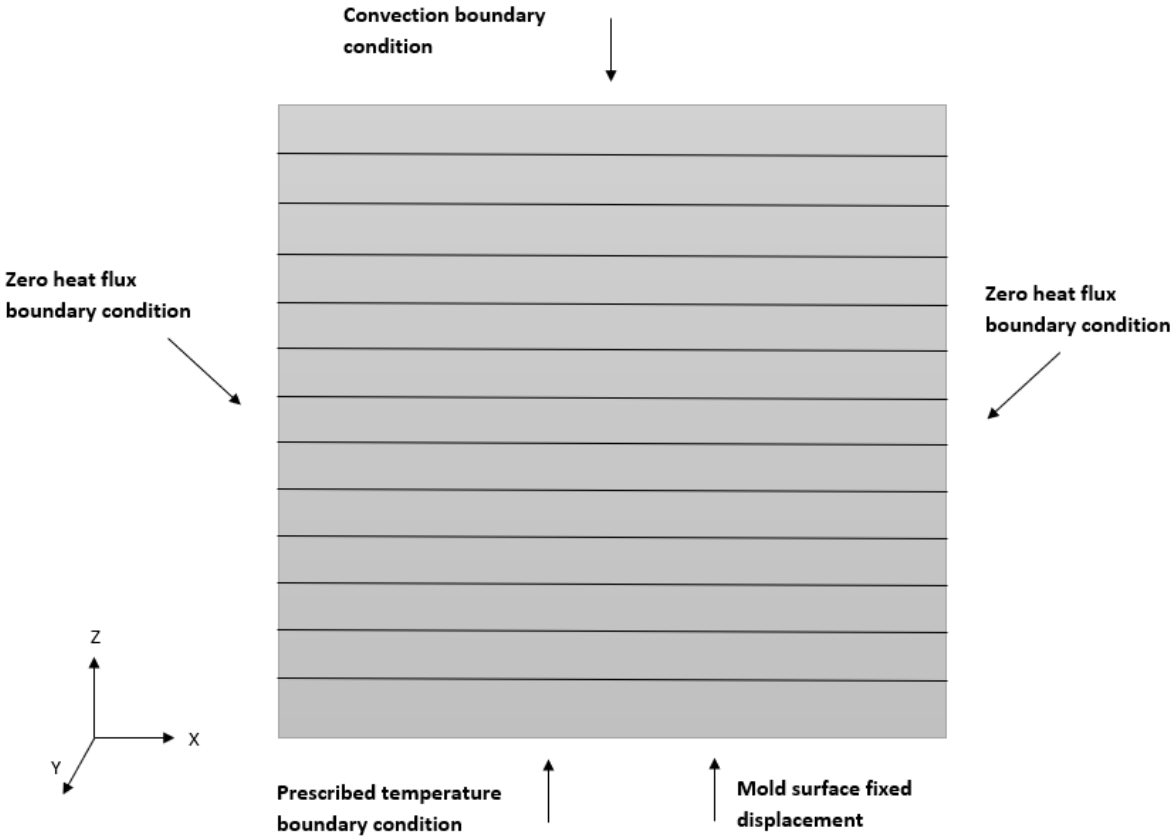

Figure 3.2: Boundary conditions applied

3.1 ABAQUS Model

This section describes how the finite element model and how the simulation is done. The temperature and stress evolution inside the laminates are calculated by using Abaqus CAE with user defined subroutines. Three different models are created for every different case (see Table 3.1). The models created are:

1) VARTM process to simulate manufacturer recommended cure cycle (model 1)
2) Additive VARTM process without using pre-cured sub-laminates (model 2)
3) Additive VARTM process by using pre-cured sub-laminates (model 3)

Manufacturing Methodology	**Total # of sub-models created**	**Calculation of temperature and stress**	**Are sub-laminates used /Are they pre-cured?**
1- MRCC	1	✓/✓	X
2-Additive Process without pre-cure	3	✓/✓	✓/X
*3-Additive Process with pre-cure**	2 or 3	✓/✓	✓/✓

Table 3.1: Difference between manufacturing processes

*Model 3 includes two different sub models, Model 3.1, and Model 3.2 (see page 21)

3.1.1 Finite Element Models

When VARTM process is considered (i.e. Model 1), only one model is needed, requiring just one input file. After the model is created, it is ready to run with the subroutines. The geometry created has a total total thickness of 31.5 mm with initial degree of cure 0.08. As shown in Figure 3.1 the MRCC is here applied as boundary condition.

The model for additive VARTM process (model 2) consists of three sub-models which enables user to solve coupled temperature-displacement problems. The first sub-model includes the first sub-laminate only. After the sub-laminate reaches the desired degree of cure, the output of the first sub-model is defined as an input for second sub-model. After predefining the first sub-laminate in the initial state, the sub-laminate which is freshly added is defined as stress and strain free state with 0.08 degree of cure. Once the second sub-laminate reaches the desired degree of cure, the same procedure is applied to the subsequent operations until cure cycle for manufacturing is completed. Figure 3.3 shows the degree of cure distribution at the beginning of second cure cycle with total of 21 mm thickness.

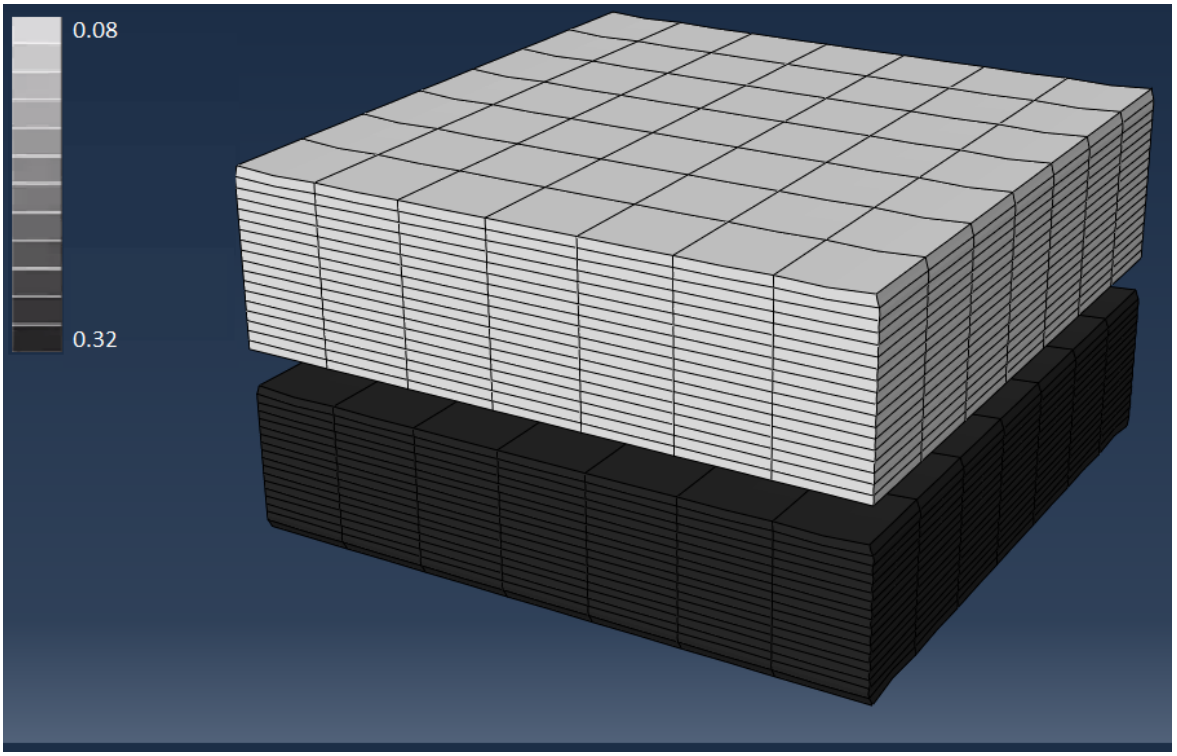

Figure 3.3 Degree of Cure Distribution at the beginning of second cure cycle (Model 2)

The model for pre-cured sub-laminates (model 3) is similar to what is done in model 2. Two different approaches have been considered in this model. First one is pre-curing each sub-laminate to desired degree of cure and, afterwards finalize curing all the sub-laminates together (Model 3.1). The second one is curing these sub-laminates on top of the other pre-cured sub-laminate one by one (Model 3.2). In this model, all the sub-laminates are first pre-cured before adding new one.Like in Model 2, the initial states of the sub-laminates are defined and input into the Model 3.1 or Model 3.2. So that these laminates are not stress and strain free and their values like degree of cure or Tg have already reached a certain value because of the previous curing operations. As a benchmark, Model 3.1 is used to compare with different manufacturing methods. Figure 3.4 shows the degree of cure distribution after first cure cycle is applied for Model 3.1.

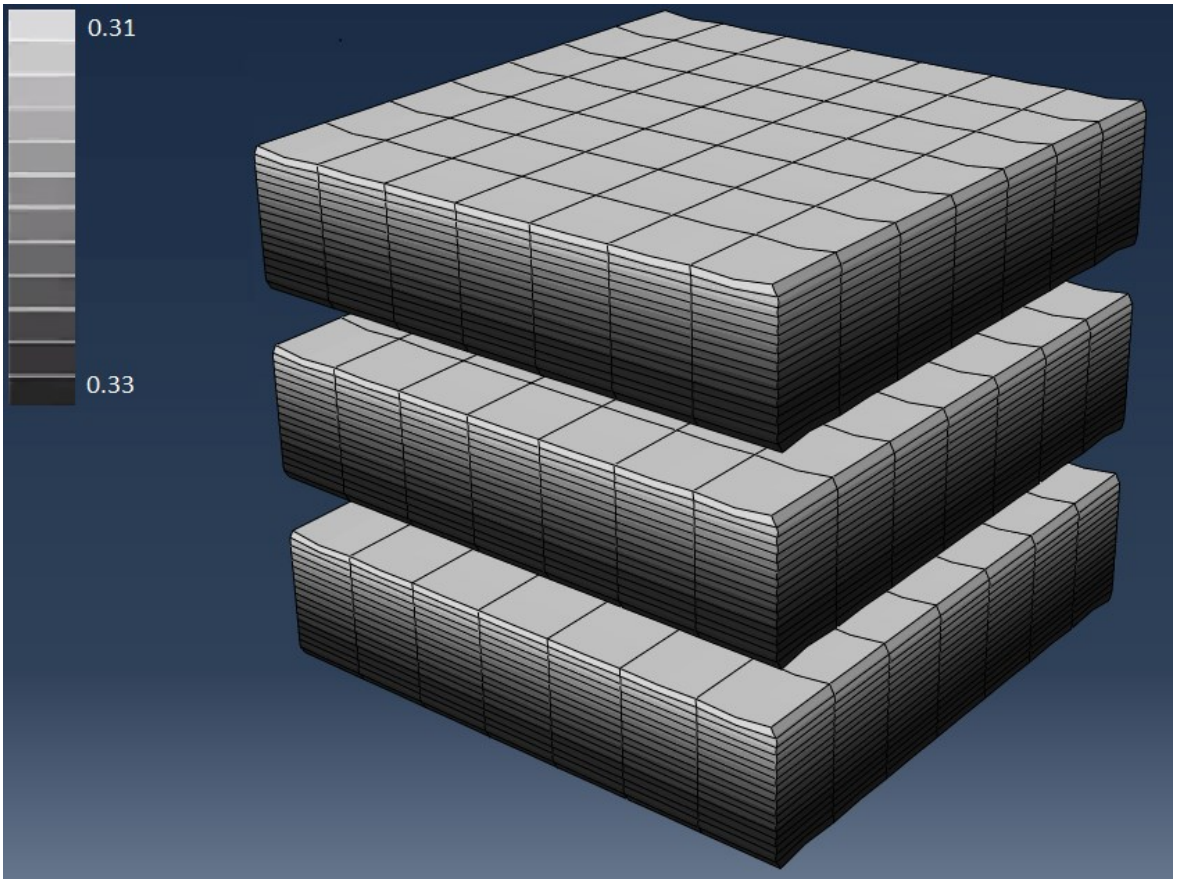

Figure 3.4 Degree of cure distribution after first cure cycle (Model 3.1)

In Figure 3.5, a representative flow chart can be seen for different type of methodologies which includes the additive process. Model 2 and Model 3 start with reaching the desired degree of cure for the first sub-laminate. The main difference starts when subsequent layers are added. In case of additive VARTM process without pre-cured sub-laminates, the new layer is defined with stress free initial conditions, while in case of additive VARTM process with pre-cured sub-laminates, new sub-laminates are imported from previous analyses.

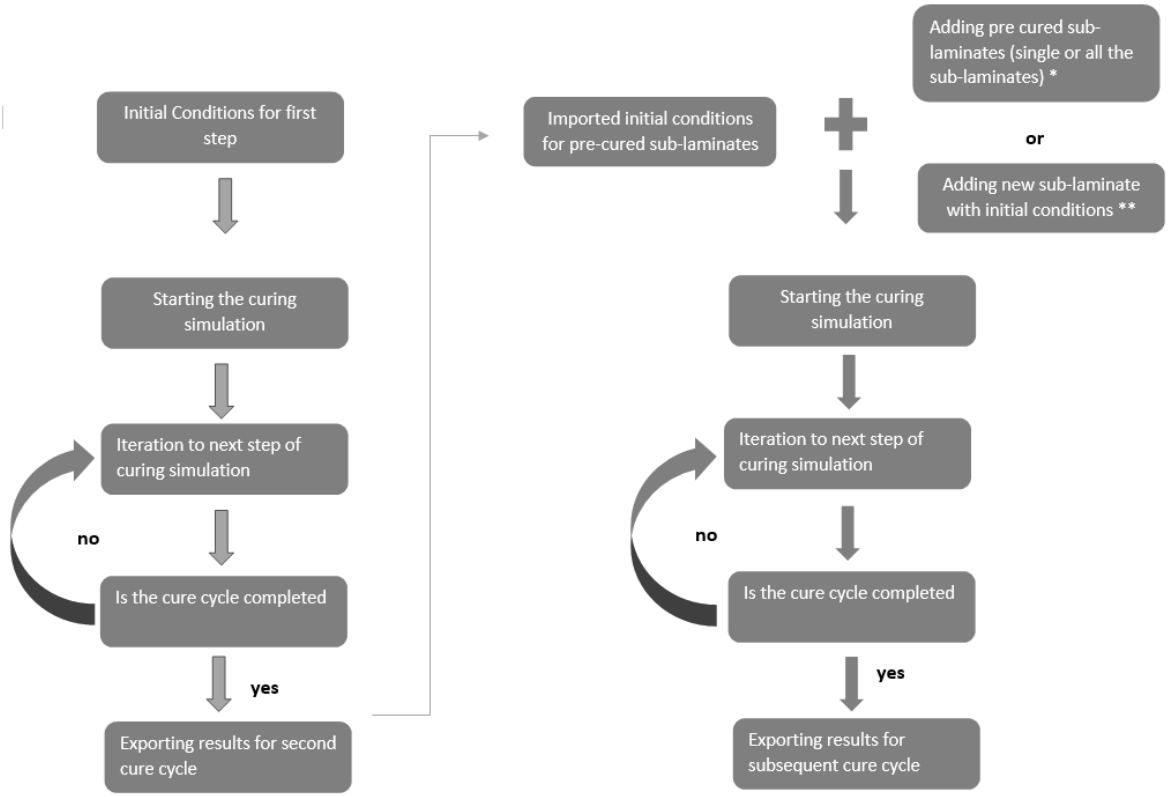

Figure 3.5 Schematic for different manufacturing (*: Model 3.1 & Model3.2, **: Model 2)

3.1.4 Mesh Convergence

A mesh convergence analysis has been conducted to decide the most time and memory efficient mesh structure. In the study, five different mesh sizes have been investigated. Mesh sizes goes from the course one to the finest one. In the mesh convergence analysis, only rectangular elements with square base are used since the overall geometry is a cube. Table 3.2 shows the different mesh densities selected for the analysis. First, element length in x and y direction is decreased. When relative error has reached a sufficient value which is 5% [68], the thickness of element is decreased. It has been decided that number three has good accuracy without increasing the computational cost excessively.

Mesh Number	Length(mm)	Thickness(mm)	Total # of elements	Relative error S11&S33 (%)
1	10.5	0.583	1134	
2	6.3	0.583	1890	1.4%-26.87%
3	4.5	0.583	2646	0.2%-10.56%
4	2.3	0.583	5292	<0.1%-1.62%
5	4.5	0.292	5292	<0.1%-1.08%

Table 3.2: Mesh Convergence Study

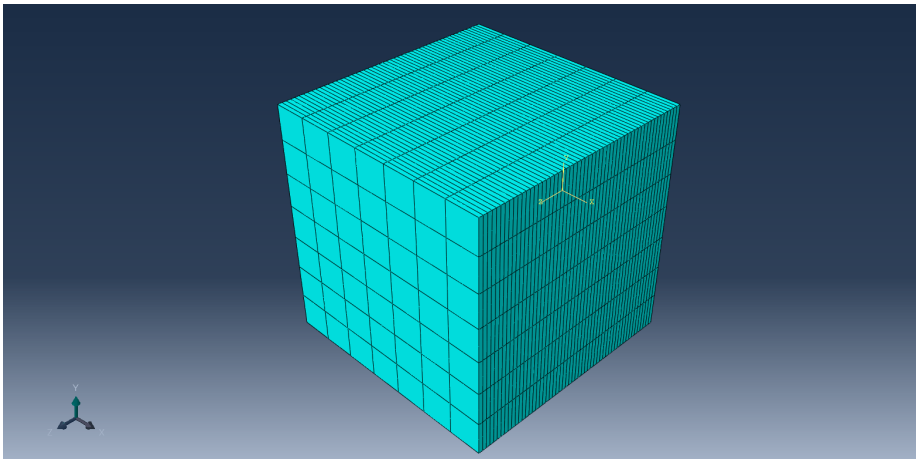

Figure 3.6: Representation of selected mesh size

3.2 Material Models

The material properties are defined as a function of degree of cure and temperature. So, in every incremental time step material properties are re-calculated. To implement changes in mechanical properties, following models are used.

3.2.1 Cure Kinetics

To calculate updated material properties, the first thing that should be calculate is the rate of degree of cure and the degree of cure itself. Here, an autocatalytic model with diffusion factor is used [70]. The equation used is:

$$\frac{d\alpha}{dt} = \frac{Ae^{-\frac{E}{RT}}}{1+e^{C(\alpha-\alpha_c-\alpha_T T)}}(1-\alpha)^n\alpha^m \qquad (3.1)$$

After the reaction rate is calculated, degree of cure is calculated by using a finite difference method. Regarding the selection of a method, here below in Figure 3.7, the result of a research conducted by Tavakol et al [84] can be seen.

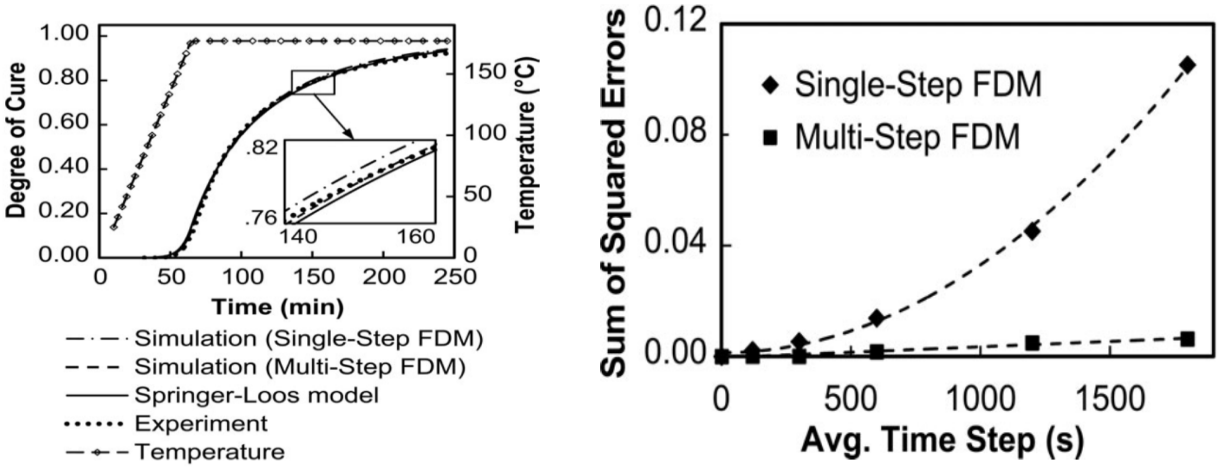

Figure 3.7: Difference Between Finite Difference Methods

The single step finite difference methods are using single degree of cure value from previous step, while multi-step finite difference methods are using multiple values from more than one previous step. Since the order is higher for multi-step finite difference methods, it can be expected them to be more accurate. However, the relative error is a function of time and since the time step in the analysis is small (max allowable time increment is 100 seconds), the error can be expected to have a low value. As a result, the effect of using multi-step finite difference method is not significant. So, in this study, implicit forward Euler's method has been used. The equation to calculate degree of cure can be defined as:

$$\alpha_{new} = \alpha + \frac{\Delta\alpha}{\Delta t}\Delta t \qquad (3.2)$$

where α is the degree of cure, Δt is the change in time, $\frac{\Delta\alpha}{\Delta t}$ is the reaction rate. Once the rate of degree of cure has been calculated, the exothermic heat due to the curing of the resin and Tg are ready to be calculated. They can be defined as:

$$\dot{Q} = \left(1 - \nu_f\right)\rho_r H_T dt \qquad (3.3)$$

$$T_g = T_{g0} + \frac{\left(T_{g\infty} - T_g\right)\lambda\alpha}{1-(1-\lambda)\alpha} \qquad (3.4)$$

where $\dot{Q}$is the instantaneous heat generation, H_T is the total reaction heat, ν_f is the fiber volume fraction, T_{g_0} and T_{g_∞} are the glass transition temperature of uncured and fully cured resin, respectively and λ is a fitting parameter between zero and one.

Parameters	Values	Units
A	681085	s^{-1}
E	59291	J/mol^{-1}
n	1.67	
m	0.12	
C	47.7	
α_c	0.77	
α_T	0.0016	$°C^{-1}$
H_T	434000	$J\ kg^{-1}$
T_{g0}	-55	°C
$T_{g\infty}$	89	°C
λ	0.476	

Table 3.3: Cure kinetics of Airstone 780E/785H epoxy resin system [64]

3.2.2 Thermal Properties

The thermal properties of the composite material depend on temperature, Tg and the degree of cure. For the epoxy resin, thermal properties are changing with these variables while thermal properties of the fiber can be variable with temperature (i.e. specific heat) or constant (i.e. thermal conductivity). The specific heat capacity of the fiber, resin and the composite can be defined as [71]:

$$c_{p,f} = A_{f_{c_p}} T + B_{f_{c_p}} \quad (3.5)$$

$$c_{p,r} = A_{r_{c_p}} T + B_{r_{c_p}} + \frac{\Delta_{rc_p}}{1+e^{C_{rc_p}(T-Tg-\sigma)}} \quad (3.6)$$

$$c_{p,c} = w_f c_{p,f} + (1 - w_f) c_{p,r} \quad (3.7)$$

where $A_{f_{c_p}}$, $B_{f_{c_p}}$, $A_{r_{c_p}}$ and $B_{r_{c_p}}$ are parameters of linear dependency for the heat capacity with temperature and subscripts f and r describes fiber or resin, respectively. Δ_{rc_p}, C_{rc_p} and σ are the strength, width and temperature change respectively to the glass

transition. The thermal conductivity of the composite material should be calculated by using the contribution from both the fiber and the resin. For a single ply the material can be considered to be transversely isotropic which leads in the result of calculation of two direction which are longitudinal direction component K_l and transverse direction K_t [64].

Thermal conductivity of the fibers, resin and composite material can be defined as [71,72,73]:

$$K_{lf} = A_{lf} \tag{3.8}$$

$$K_{tf} = A_{tf} \tag{3.9}$$

$$K_r = a_{Kr}T\alpha^2 - b_{Kr}T\alpha - c_{Kr}T - d_{Kr}\alpha^2 + e_{Kr}\alpha + f_{Kr} \tag{3.10}$$

$$K_l = \nu_f K_{lf} + (1 - \nu_f)K_r \tag{3.11}$$

$$K_t = \nu_f K_r \left(\frac{K_{tf}}{K_r} - 1\right) + K_r \left(\frac{1}{2} - \frac{K_{tf}}{2K_r}\right) + K_r \left(\frac{K_{tf}}{2K_r} - 1\right) \sqrt{\nu_f^2 - \nu_f + \frac{\left(\frac{K_{tf}}{K_r}+1\right)^2}{\left(\frac{2K_{tf}}{K_r}-2\right)^2}} \tag{3.12}$$

where K_{lf} and K_{tf} are thermal conductivities of fiber in longitudinal and transverse direction. K_r is thermal conductivity of resin, A_{lf} and A_{tf} are longitudinal and transverse dependency parameters for thermal conductivity of fiber.

Parameters	Values	Units
A_{fcp}	0.0014	J g^{-1} °C^{-2}
B_{fcp}	0.841	J g^{-1} °C^{-1}
A_{rcp}	0.0025	J g^{-1} °C^{-2}
B_{rcp}	1.80	J g^{-1} °C^{-1}
Δ_{rcp}	-0.25	J g^{-1} °C^{-1}
C_{rcp}	1.10	°C^{-1}
σ	16.5	°C
K_{lf}	1.03	W m^{-1} °C^{-1}
K_{tf}	1.03	W m^{-1} °C^{-1}
a_{Kr}	0.0008	W m^{-1} °C^{-2}
b_{Kr}	-0.0011	W m^{-1} °C^{-2}
c_{Kr}	-0.0002	W m^{-1} °C^{-2}
d_{Kr}	-0.0937	W m^{-1} °C^{-1}
e_{Kr}	0.22	W m^{-1} °C^{-1}
f_{Kr}	0.12	W m^{-1} °C^{-1}
ρ_f	2580	kg m^{-3}
ρ_r	1105	kg m^{-3}

Table 3.4: Thermal properties of the glass fibres and Airstone 780E/785H epoxy resin system [64]

where E_r and E_{lf} are resin and longitudinal fiber modulus, ν_r, ν_{12f} and ν_{12} are the Poisson's ratio of the resin, Poisson's ratio of fiber and composite in-plane direction, respectively.

Lastly, the resin shrinkage should be defined to complete the thermal model. The linear shrinkage of the resin is 1.9% that corresponds to a 5.6% volumetric shrinkage [75]. An isotropic shrinkage of the composite can be modelled as following [75]:

$$\gamma_r = \gamma_\alpha \alpha \qquad (3.13)$$

$$\gamma_l = \frac{(1-\nu_f)E_r\gamma_r}{(1-\nu_f)E_r+\nu_f E_{lf}} \quad (3.14)$$

$$\gamma_t = (1-\nu_f)\gamma_r + (1-\nu_f)\gamma_r\nu_r - \nu_{12}\gamma_{12} \quad (3.15)$$

where γ_r, γ_l and γ_t are shrinkage of resin, shrinkage of system in fiber and transverse direction, ν_r, and ν_{12} are the Poisson's ratio of the resin, and composite in-plane direction, respectively.

	Parameters	Values	Units
	a_{lf}	5e-06	°C^{-1}
	a_{tf}	5e-06	°C^{-1}
	a_{glass}	6e-05	°C^{-1}
	a_{rub}	1.7e-04	°C^{-1}
	Cm	0.4	°C^{-1}
	σ_m	10.2	°C
	γ_α	0.019	

Table 3.5: Expansion and shrinkage properties Airstone 780E/785H epoxy resin system [64]

3.2.3 Mechanical Properties

While defining the mechanical properties of the composite material, Young's Modulus and Shear Modulus of the material can be defined by considering contributions from resin and the fiber [75]. Here in this thesis, the suggested formula by Chamis [76] is used. The longitudinal and transverse modulus can be described as:

$$E_r = E_{rub} + \frac{(E_{glass}+E_{glassT}\times T-E_{rub})}{1+e^{C_m(T-T_g-\sigma_m)}} \quad (3.16)$$

$$E_l = \nu_f E_{lf} + (1-\nu_f)E_r \quad (3.17)$$

$$E_t = \frac{E_r}{1-\sqrt{(\nu_f)}\left(1-\frac{E_r}{E_{tf}}\right)} \quad (3.18)$$

where v_f is the fibre volume fraction, E_{lf} and E_{tf} is the Young's modulus of fibre in longitudinal direction and transverse direction, E_r is the Young's modulus of the resin. Shear modulus of the composite can be defined as:

$$G_{12} = G_{13} = G_{23} = \frac{G_r}{1-\sqrt{v_f}\left(1-\frac{G_r}{G_{12f}}\right)} \quad (3.19)$$

$$G_{23} = \frac{G_r}{1-\sqrt{v_f}\left(1-\frac{G_r}{G_{23f}}\right)} \quad (3.20)$$

where G_r, G_{12_f} and G_{23_f} are the resin and fiber shear modulus longitudinal and transverse, respectively. In this study, since G_{12_f} and G_{23_f} have the same value, three components of shear modulus are equal. Lastly, in plane Poisson's ratio can be defined as:

$$v_{12} = v_f v_{12_f} + (1 - v_f)v_r \quad (3.21)$$

where v_r is the resin volume fraction and v_{12_f} Poisson's ratio of the fiber in plane direction.

The thermal expansion of the composite can be implemented in longitudinal and transverse direction as well [74].

$$a_r = a_{rub} + \frac{(a_{glass} - a_{rub})}{1+e^{C_m(T-T_g-\sigma_m)}} \quad (3.22)$$

$$a_l = \frac{(1-v_f)E_r a_r + v_f E_{lf} a_{lf}}{(1-v_f)E_r + v_f E_{lf}} \quad (3.23)$$

$$a_t = (1 - v_f)a_r + v_f a_{tf} + (1 - v_f)a_r v_r + v_{12f} a_{lf} v_f - v_{12} a_l \quad (3.24)$$

where E_r and E_{lf} are resin and longitudinal fiber modulus, v_r, v_{12f} and v_{12} are the Poisson's ratio of the resin, Poisson's ratio of fiber and composite in-plane direction, respectively.

Parameters	Values	Units
E_{lf}	73.1	GPa
E_{tf}	73.1	GPa
G_{12f}	30	GPa
G_{23f}	30	GPa
ν_{12f}	0.22	
E_{glass}	4.61	GPa
E_{glassT}	-0.012	GPa °C^{-1}
E_{rub}	0.04	GPa
ν_{glass}	0.35	
ν_{rub}	0.5	
C_m	0.4	°C^{-1}
σ_m	10.2	°C

Table 3.6: Mechanical Properties of glass fibers and Airstone 780E/785H epoxy resin system [75]

3.2.4 Elastic Thermal and Chemical Strain

During the curing process, contributions from three different effects are included in the calculation of strain. They are elastic, thermal, and chemical strain. Elastic, thermal, and chemical strain and their derivatives are defined in the subroutine. These variables can be defined as [68]:

Thermal Strain

$$d\varepsilon_{t_l} = a_l \Delta T \quad (3.25)$$

$$\varepsilon_{t_{l_{new}}} = \varepsilon_{t_l} + d\varepsilon_{t_l} \quad (3.26)$$

$$d\varepsilon_{t_t} = a_t \Delta T \quad (3.27)$$

$$\varepsilon_{c_{t_{new}}} = \varepsilon_{t_t} + d\varepsilon_{t_t} \quad (3.28)$$

Chemical Strain

$$d\varepsilon_{c_l} = -\gamma_l \quad (3.29)$$

$$\varepsilon_{c_{l_{new}}} = \varepsilon_{c_l} + d\varepsilon_{c_l} \quad (3.30)$$

$$d\varepsilon_{c_t} = -\gamma_t \quad (3.31)$$

$$\varepsilon_{t_{t_{new}}} = \varepsilon_{c_t} + d\varepsilon_{c_t} \quad (3.32)$$

Elastic Strain

$$\varepsilon_{e_{new}} = \varepsilon_e + \left(d\varepsilon_e - (d\varepsilon_t + d\varepsilon_c)\right) \quad (3.33)$$

6 directions in total, 3 normal and 3 in-plane.

Once these increments are calculated in every step, they are recorded in solution dependent variables, and they can be seen in the first 18 solution dependent variables (SDVs). First six one defines elastic strain in normal direction and in-plane direction. Following 6 defines thermal strain values and the last six SDVs are defining chemical strain. It should be noted that thermal and chemical strain have values in normal direction only. So, in-plane directions are defined as zero and they have no contribution.

3.2.5 Stiffness Matrix

After the strains are defined, the value of stresses can be found once the stiffness matrix is also defined. Since composite structures is not isotropic, the way stiffness matrix is defined is a bit complex. The definition of the stiffness matrix is taken from Skrzypek [77]. An orthotropic Hooke's compliance matrix structure is used. Below in Figure 3.8., the conventional unit cells of space lattices, compliance matrix and example of composite structure can be seen for the selection.

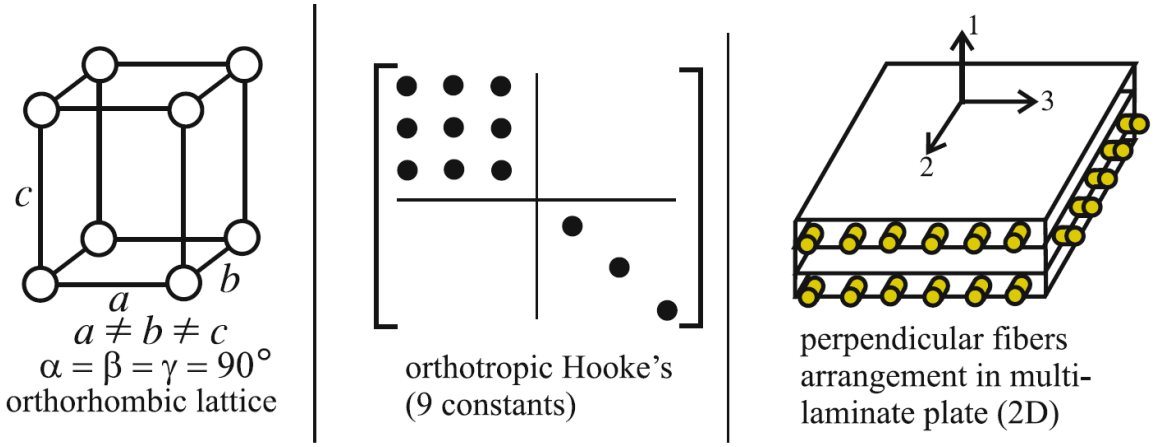

Figure 3.8: Classification of selected composite [77]

Once the matrix is selected in can be defined as [68]:

$$\begin{pmatrix} \frac{1-\nu_{23}\nu_{32}}{\delta}E1 & \frac{\nu_{12}+\nu_{13}\nu_{32}}{\delta}E2 & \frac{\nu_{13}+\nu_{12}\nu_{23}}{\delta}E3 & 0 & 0 & 0 \\ \frac{\nu_{12}+\nu_{13}\nu_{32}}{\delta}E2 & \frac{1-\nu_{13}\nu_{31}}{\delta}E2 & \frac{\nu_{23}+\nu_{21}\nu_{13}}{\delta}E3 & 0 & 0 & 0 \\ \frac{\nu_{13}+\nu_{12}\nu_{23}}{\delta}E3 & \frac{\nu_{23}+\nu_{21}\nu_{13}}{\delta}E3 & \frac{1-\nu_{12}\nu_{21}}{\delta}E3 & 0 & 0 & 0 \\ 0 & 0 & 0 & \frac{G_r}{1-\sqrt{\nu_f}\left(1-\frac{G_r}{G_{12_f}}\right)} & 0 & 0 \\ 0 & 0 & 0 & 0 & \frac{G_r}{1-\sqrt{\nu_f}\left(1-\frac{G_r}{G_{12_f}}\right)} & 0 \\ 0 & 0 & 0 & 0 & 0 & \frac{G_r}{1-\sqrt{\nu_f}\left(1-\frac{G_r}{G_{23_f}}\right)} \end{pmatrix}$$

where:

$$\delta = 1 - \nu_{12}\nu_{21} - \nu_{13}\nu_{31} - \nu_{23}\nu_{32} - \nu_{12}\nu_{23}\nu_{31} - \nu_{21}\nu_{32}\nu_{13} \quad (3.34)$$

$$\nu_{12} = \nu_f \nu_{12_f} + (1-\nu_f)\nu_r \quad (3.35)$$

$$\nu_{13} = \nu_{12} \quad (3.36)$$

$$\nu_{23} = \frac{E_2}{2G_{23}} - 1 \quad (3.37)$$

$$\nu_{21} = \frac{E_2/E_1}{\nu_{12}} \quad (3.38)$$

$$\nu_{31} = \frac{E_3/E_1}{\nu_{13}} \quad (3.39)$$

$$\nu_{32} = \frac{E_3/E_2}{\nu_{23}} \quad (3.40)$$

Where E_1 is the longitudinal modulus of the composite and $E_2 \& E_3$ are the modulus in transverse direction.

4 Results and Discussion

This section describes the results obtained. The results aim to answer the research questions while understanding the mechanisms behind them. The first part is explaining the results in stresses longitudinal & transverse direction, and modulus. The second part is comparing different types of manufacturing methods.

4.1 Results of Thermo-Mechanical Analysis

Figure 4.1 reports the resin modulus development when MRCC is applied. In the literature, it can be found that until the gelation point Young's Modulus does not develop and after the gelation point, it increases significantly [75]. In this study, gelation point is estimated by identifying the region at which the resin modulus starts building up. This occurs at about 140 minutes and corresponds to 0.68 degree of cure [75]. This transition happens at different times for different manufacturing processes. The second important point for the development of Young's Modulus is vitrification. Figure 4.2 shows the vitrification point taken from a single infusion case in the middle section. At 380 minutes, the temperature of resin gets equal to the glass transition temperature and vitrification happens. After vitrification, it can be considered that the development of the Young's Modulus is linear for this resin system.

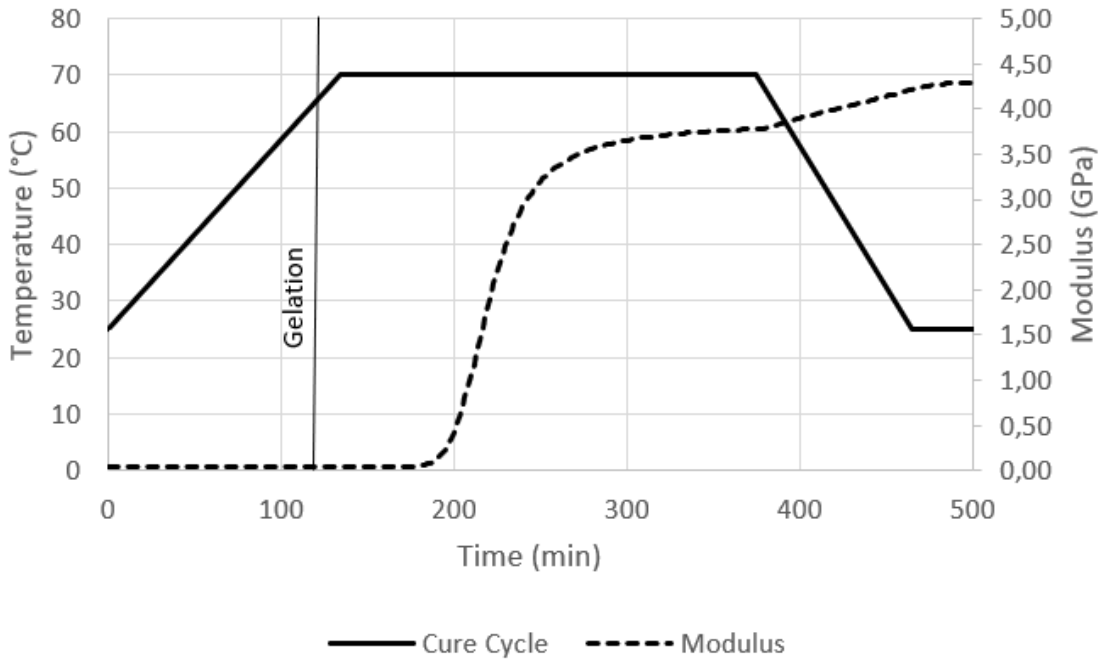

Figure 4.1: Development of modulus

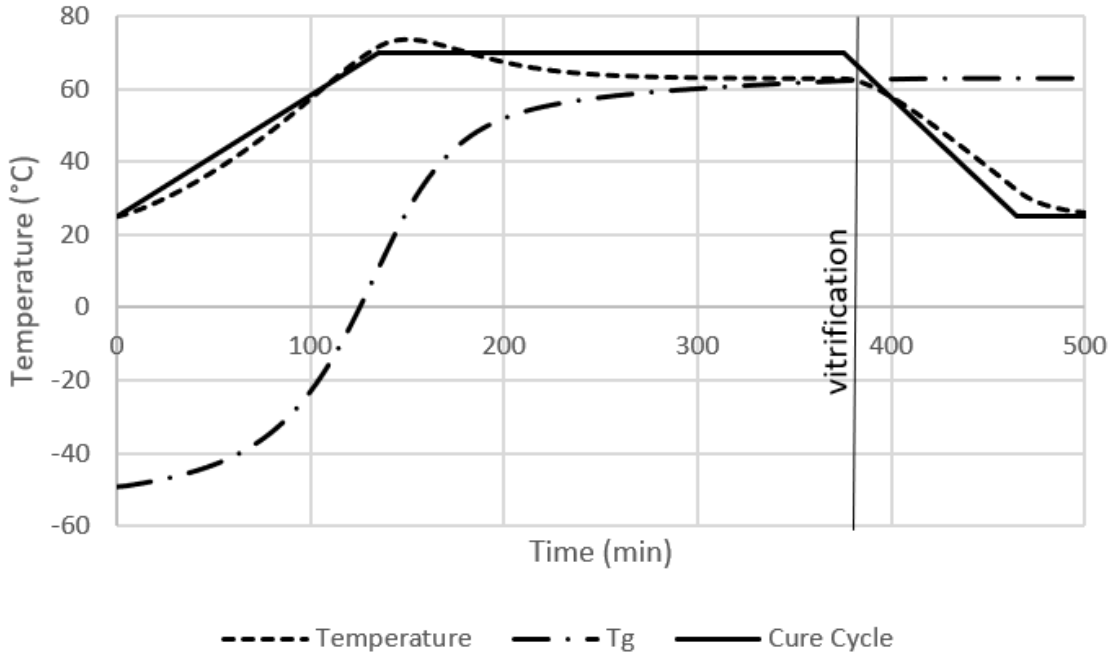

Figure 4.2: Development of Tg

4.1.1 Temperature Overshoot

The mechanism behind cure kinetics is described in section 2.4. Since curing of the resin is an exothermic reaction, higher temperature values compared to dwell temperature is expected in some regions of the structure analyzed. The thermal conductivity through thickness is very low and heat generated cannot dissipate easily. In this study, since the top surface is subjected to free convection, the highest temperature overshoot is expected in the middle region. Figure 4.3 shows the temperature profile in the middle and top section when MRCC is applied (Model 1). For the case analyzed, it is noticed that while temperature overshoot is observed in the middle section, the top surface does not exceed the dwell temperature due to natural convection. The temperature difference between middle and top surface is five to seven degrees depending on the manufacturing method.

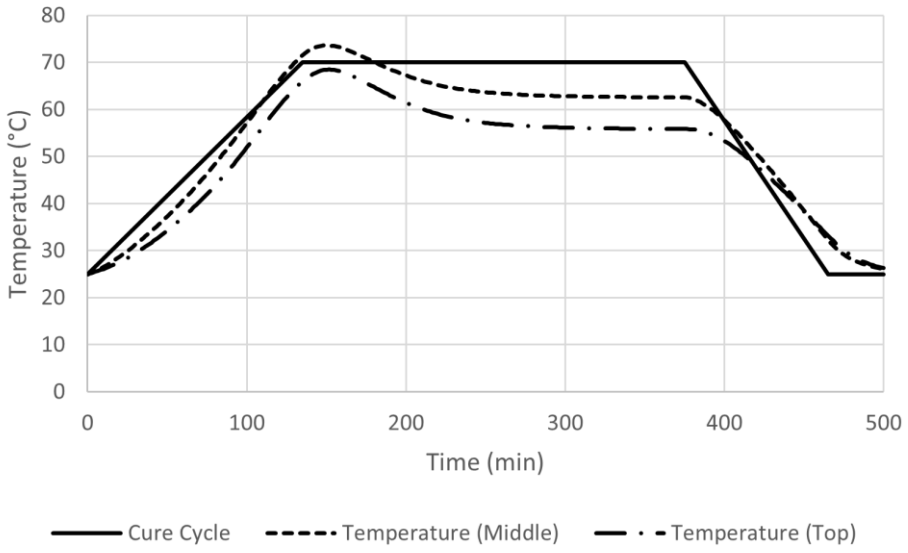

Figure 4.3 Temperature Profile at the Middle and Top (Model 1)

4.1.2 Cure Induced Stress in Longitudinal Direction

The sources of residual stresses are mentioned in section 2. In this study since the interaction between the tool and the part is not included, the development of residual stresses is due to the curing process only. The nature of the curing process

generates different residual stresses during the process. During the heating, in fiber direction the material expands which creates tensile stresses, and during the process is shrinkage dominated which generates compressive stress. Figure 4.4 shows the development of stress in fiber direction (a) during the cure cycle when MRCC is applied (i.e. Model 1) and development of stress in fiber-direction and the modulus evolution (b). It can be seen that during heating, tensile stresses develop. However, due to the low value of the modulus, they are negligible. In literature up to this point material is considered stress-free status [79]. At about 140 min, as soon as the modulus of the resin is high enough to carry stress, compressive stress starts to develop. The modulus of resin increases from 40 MPa to 4.3 GPa at the end of process. At 375 min cool down starts and development of residual stress is due to the cooldown from this point onward [75].

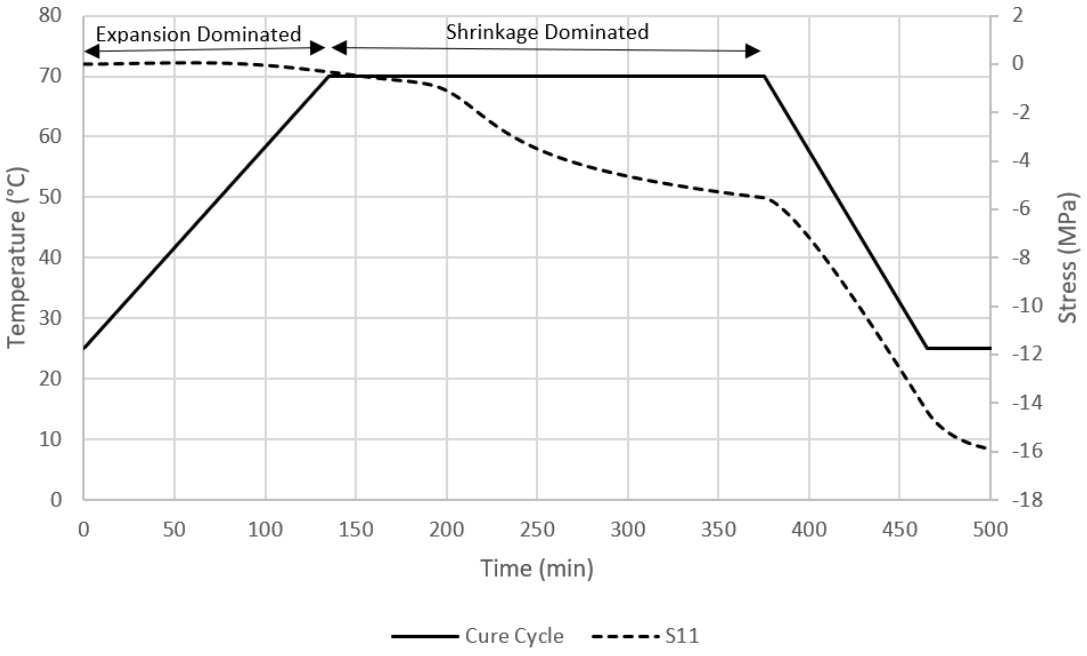

a)

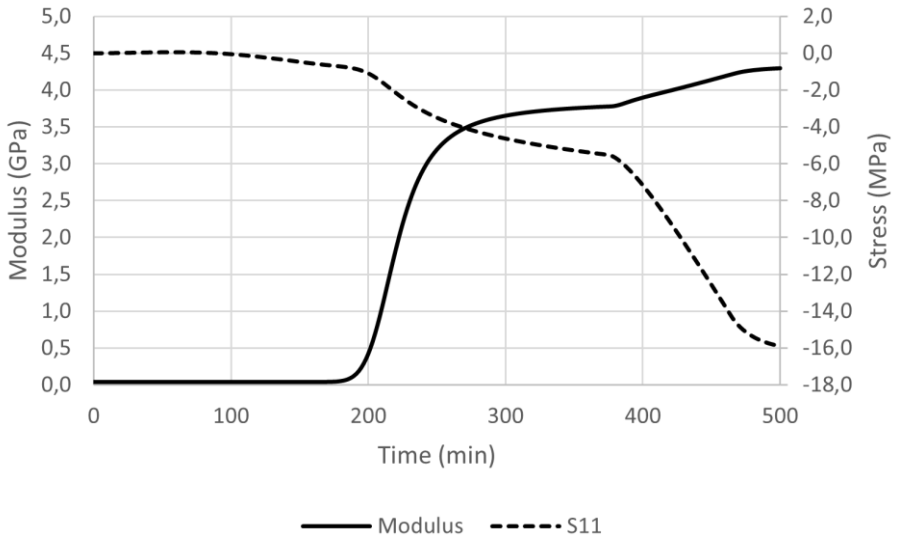

b)

Figure 4.4: S11 Evolution at the middle a) with cure cycle b) with Modulus

4.1.3 Stress in Transverse Direction

Cure induced residual stress evolution in transverse directions is examined for two directions, in-plane and through thickness (S22 and S33). The magnitude and behavior of S22 is similar to stress in fiber direction but mirrored. Figure 4.5 shows the result of S22 when MRCC is applied (i.e. Model 1). The difference compared to fiber direction is, in expansion dominated zone, instead of tensile stress, compressive stress develops and in shrinkage dominated zone instead of compressive stress, tensile stress develops.

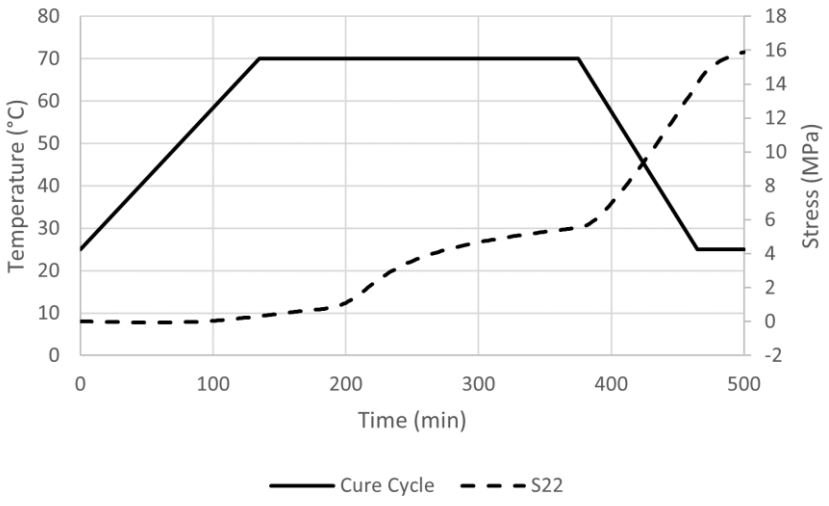

a)

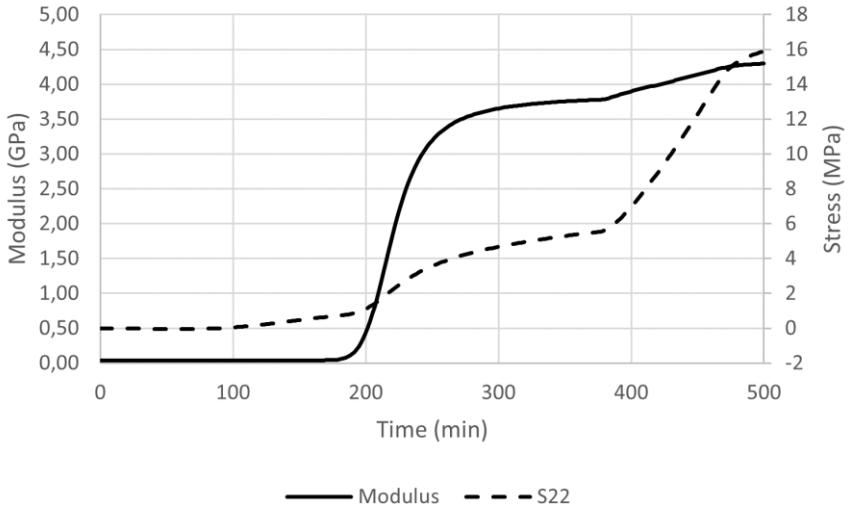

b)

Figure 4.5: S22 Evolution at the middle a) with cure cycle b) with Modulus

Figures 4.6 and 4.7 show the difference between the behavior of stress at the top and in middle in transverse through thickness direction when MRCC is applied (i.e. Model 1). Like the longitudinal direction, before development in the modulus of the resin, the material cannot bear stresses, so they remain almost stress-free. Once gelation occurs both at the middle and at the top tensile stresses start to develop.

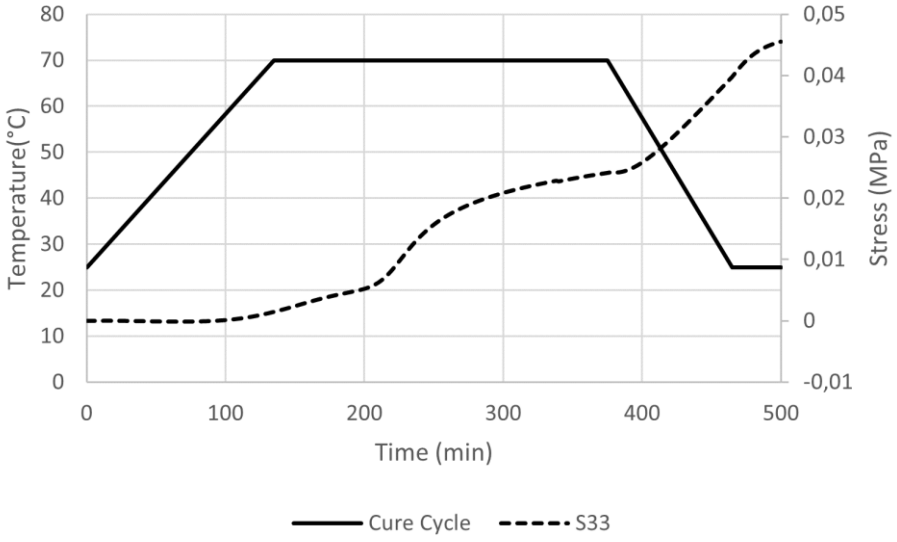

a)

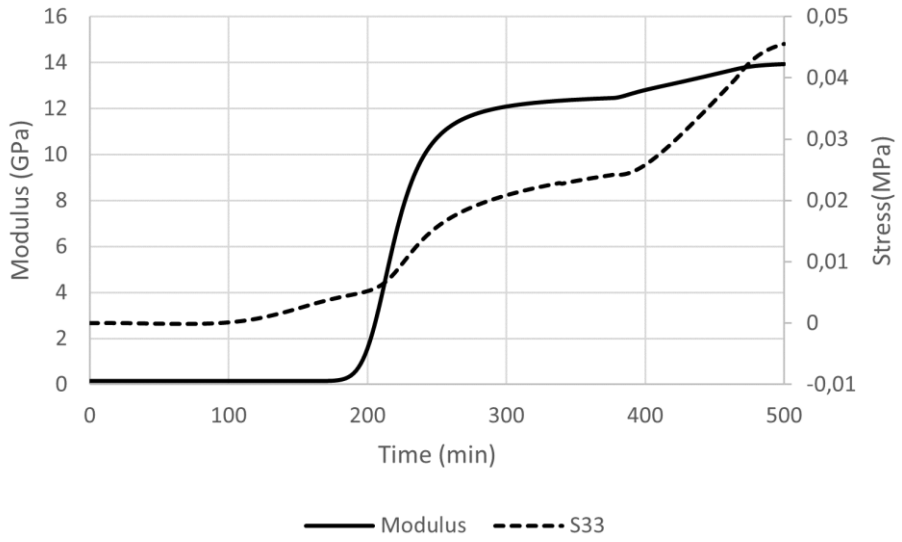

b)

Figure 4.6: S33 Evolution at the top a) with cure cycle b) with modulus

At the top, S33 is able to develop tensile stresses. On the other hand, at the middle, due to the influence of the other layers and the presence of fixed displacement at tool side, material is not free to expand. In the early stages of dwell, tensile stress develops, after short time due to effect of other layers compressive stress develops until end of dwell duration. The evolution of S33 at top 5 layers can be seen in the Figure 4.8 for the case when MRCC is applied (i.e. Model 1). The vertical line shows the beginning of cool down. The influence of surrounding layers disappear with vicinity to the top.

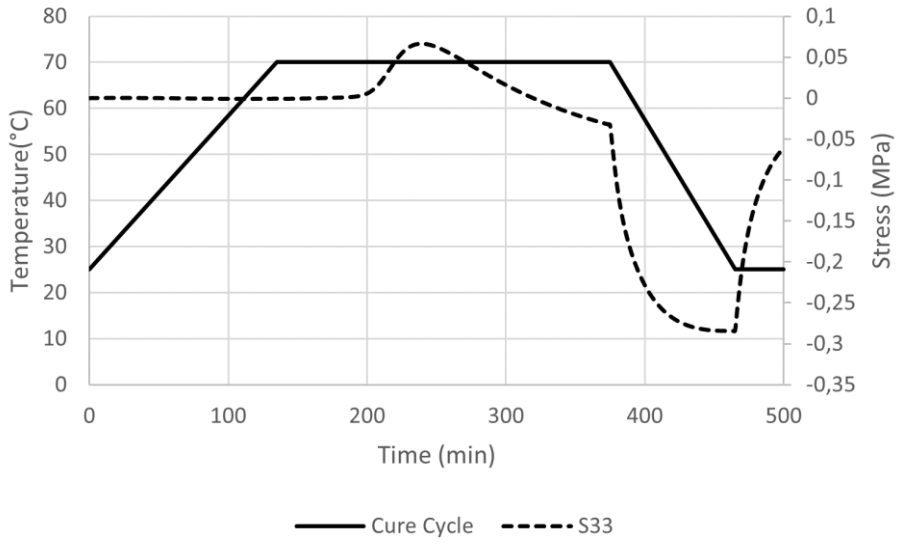

a)

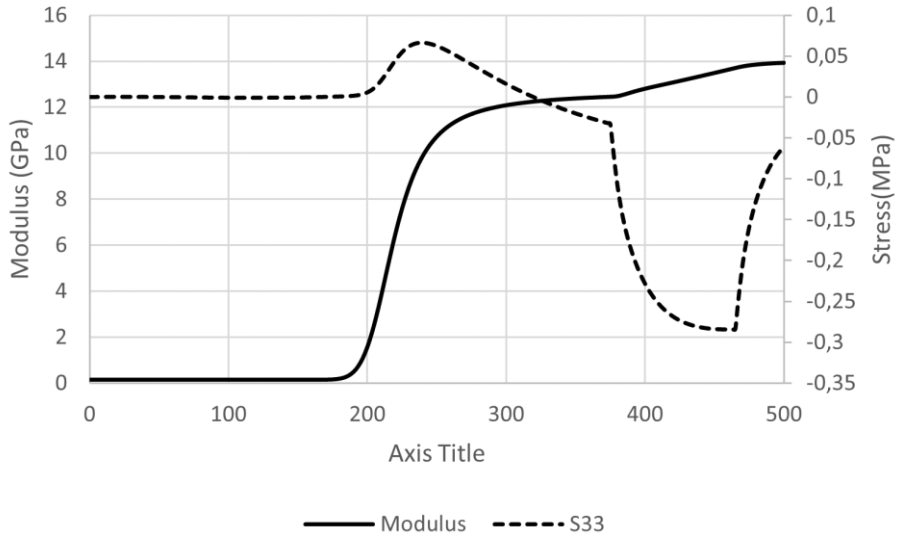

b)

Figure 4.7: S33 Evolution at middle a) with cure cycle b) with modulus

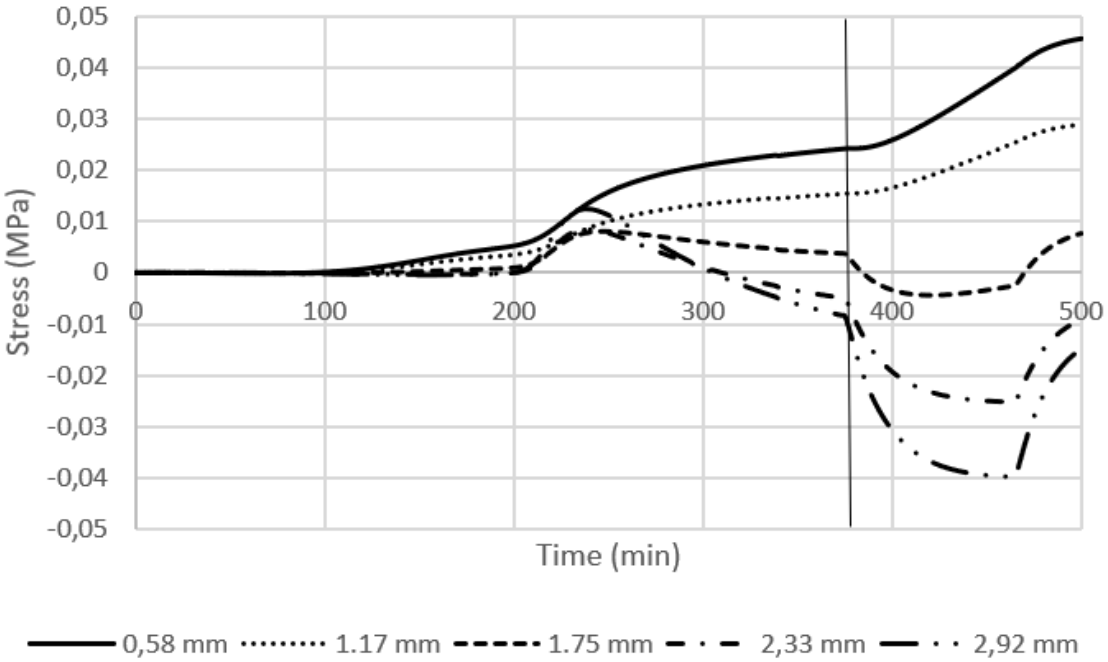

Figure 4.8: Evolution of S33 at top five layers

It is noticed that through thickness direction the magnitude of stress is approximately two order smaller than in-plane directions. The reason for this is material is able to expand/shrink in thickness direction more freely compared to in-plane directions due to 0/90 fiber layup.

4.2 Effect of Manufacturing Methods

Here in this section, the effect of different manufacturing methods is discussed. It has been shown that, during manufacturing of thick components, MRCC is not an optimal cure cycle and different approaches can reduce residual stresses on the component [34-36,80-82]. The additive process with and without pre-cured sub-laminates (0.32 pre-cure level) are used to lower stresses at the end of process.

Manufacturing Methodology	Temperature Overshoot/ Undershoot (°C)	Reduction in °C	Stress at the end of dwell (MPa)	Stress Reduction in MPa / %
1- Model 1	3.67	-	5.52	-
2- Model 2	0.76	2.91	5.44	0.08 / 1.5%
3- Model 3.1	-0.78	4.45	5.16	0.36 / 6.5%

Table 4.1: Temperature and cure induced residual stress results for different manufacturing methods at the middle

Manufacturing Methodology	Temperature Overshoot/ Undershoot (°C)	Reduction in °C	Stress at the end of dwell (MPa)	Stress Reduction in MPa / %
1- Model 1	-2.14	-	5.20	-
2- Model 2	-4.98	2.84	5.04	0.16 / 3.1%
3- Model 3.1	-7.44	5.30	4.80	0.40 / 7.7%

Table 4.2: Temperature and cure induced residual stress results for different manufacturing methods at the top

Table 4.1 and Table 4.2 show the temperature overshoot and cure induced residual stresses for three different manufacturing methods (i.e. Model 1, Model 2 & Model 3.1) at the middle and top. In temperature overshoot/undershoot section, the difference between maximum temperature reached during cure cycle and dwell temperature (70^{o}C) is presented. Positive values refer to temperature overshoot while negative values refer to undershoot. In the stress section, cure induced residual stress in fiber direction is presented. Reductions in temperature and stress are compared against MRCC. The results are taken when cool down starts because it is observed that the benefit gained from different types of manufacturing is not preserved if 0.5^{o}C/min cool down rate is used. The selection of cool down rate should be optimized depending on manufacturing method and level of pre-cure. In the middle section, by using the additive VARTM process without pre-curing temperature overshoot decreases by 2.91^{o}C while the additive VARTM process with pre-curing prevents temperature overshoot to occur at the middle by reducing temperature overshoot by 4.45 ^{o}C. At the top due to the effect of convection, a

temperature undershoot occurs by 2.14 ^{o}C to 7.44 ^{o}C whilst a temperature reduction of 2.84 ^{o}C and 5.30 ^{o}C is recorded for Model 2 and Model 3.1, respectively. For Model 2 and Model 3.1 the Tg and degree of cure of the components increases during the intermediate cure cycles. For these models, since the degree of cure is higher than Model 1 when the final cure cycle step started, a part of the exothermic reaction is already completed and there is less energy remaining that is going to contribute to the temperature overshoot. As temperature overshoot decreases, the effect of thermal strain also decreases according to equations 3.25 & 3.26 since the temperature gradient is going to be lower overall during the cure cycle. It can be seen that, reduction in temperature overshoot decreases residual stresses generated during curing process. Additive VARTM processes without and with pre-cure (Model 2 & Model 3.1) decreases the stress generated by 1.5% and 6.5% respectively at the middle and 3.1% and 7.7% at the top compared to MRCC (i.e. Model 1).

In case of manufacturing thicker components, effect of additive VARTM process becomes more significant. Figure 4.9 shows the reduction in temperature and residual stress generated in fiber direction for 94.5 mm thick component at the middle for Model 3.1. In case of manufacturing a three times thicker component (i.e. root insert for wind turbine blades) with same conditions, temperature overshoot decreases from 29.8 ^{o}C to 9.6 ^{o}C and this decrease leads a reduction in cure induced residual stresses. When cool down starts, stress in fiber direction reduces from 7.99 MPa to 5.52 MPa and at the end of cool down it reduces from 18.9 MPa to 16.6 MPa. These reductions correspond 31.7% and 12.2%, respectively.

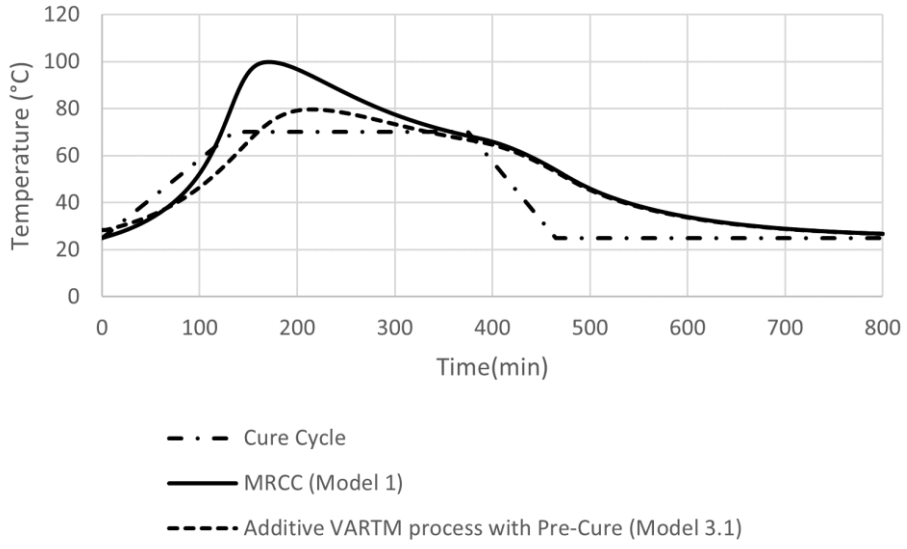

a)

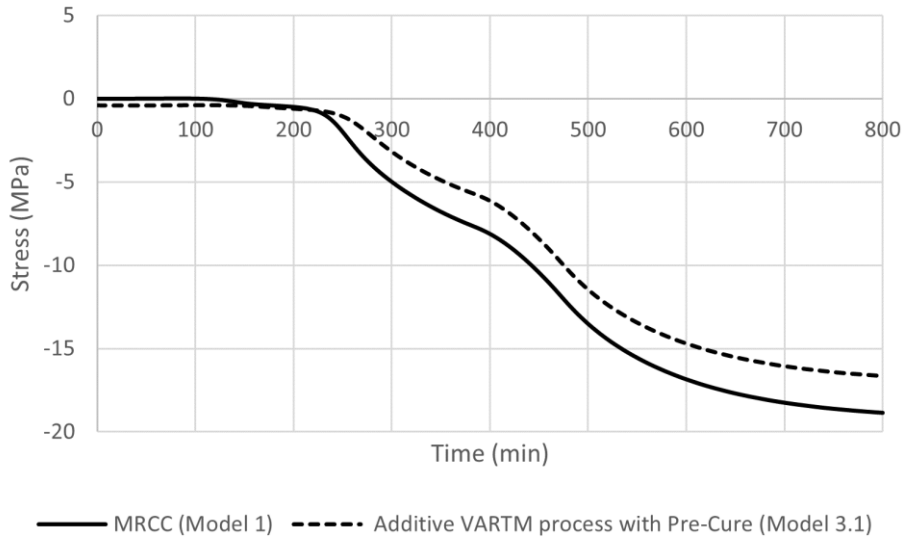

b)

Figure 4.9: Results for the 94.5mm thick component at the middle a) temperature evolution b) stress generated

4.2.2. Effect of Pre-Cure Level

The effect of pre-cure level is examined for Model 3.1 and Model 3.2 for 31.5 mm thickness. Pre-cure level of sub-laminates is an important variable since it is directly related to internal heat which is going to be reduced in the final cure cycle. As the level of pre-cure increases, less heat is produced during the final cure cycle, and it contributes to the reduction of temperature overshoot. In this analysis a harsher cure cycle is used with a ramp rate of 1°C/min to distinguish the effect of pre-cure level better. Table 4.3 and Table 4.4 shows the effect of changing pre-cure level on the temperature overshoot and cure induced stress in fiber direction for Model 3.1. At the middle, a 0.25 pre-cure level decreases the temperature overshoot by 4.09°C, from 10.38°C to 6.29°C, with respect to MRCC while 0.32 and 0.5 pre-cure levels provide further reduction by 6.80°C and 12.19°C, respectively. At top section, while 0.25 level of pre-cure experiences a temperature overshoot, increased pre-cure levels prevent temperature overshoot to occur.

Level of pre-cure	**Temperature Overshoot/ Undershoot (°C)**	**Reduction in °C**	**Stress at the end of dwell (MPa)**	**Stress Reduction in MPa / %**
1- MRCC	10.38	-	5.77	-
2- 0.25	6.29	4.09	5.54	0.23 / 4.0%
3- 0.32	3.58	6.80	5.41	0.36 / 6.2%
4- 0.5	-1.81	12.19	5.32	0.45 / 7.8%

Table 4.3: Temperature and cure induced residual stress results for different level of pre-cures at the middle (Model 3.1)

Level of pre-cure	**Temperature Overshoot/ Undershoot (°C)**	**Reduction in °C**	**Stress at the end of dwell (MPa)**	**Stress Reduction in MPa / %**
1- MRCC	5.67	-	5.42	-
2- 0.25	1.29	4.38	5.21	0.21 / 3.9%
3- 0.32	-2.10	7.77	5.08	0.34 / 6.3%
4- 0.5	-8.51	14.18	4.93	0.49 / 9.1%

Table 4.4: Temperature and cure induced residual stress results for different level of pre-cures at the top (Model 3.1)

It should be pointed out that as the level of pre-cure increases, the material does not experience temperature overshoot due to the influence of natural convection at the top surface. This might bring a question related to the degree of cure at the end of the process. It is found that at the end of the analysis, all three cases result in around 0.88 with a 0.57% difference. Therefore, stress gained due to chemical reaction is similar for the three cases examined. The effect of a lower temperature peak can be seen in the stress values reached in Table 4.3 and Table 4.4. At the middle, 0.25 level of pre-cure provides 4.0% reduction in stress in fiber direction, while 0.32 and 0.5 level of pre-cure provide 6.2% and 7.8% reduction, respectively. At the top, benefit is 3.9%, 6.3% and 9.1% for pre-cure levels 0.25, 0.32 and 0.5, respectively.

In the case of Model 3.2, similar to Model 3.1 the temperature overshoot decreases as expected. It should be noted that when the first and second sub-laminates are curing during the second cure cycle, the third sub-laminate which is going to be added at the final cycle, is held at room temperature. For third sub-laminate, curing of resin continued but at a lower rate. Table 4.5 and Table 4.6 show the temperature overshoot and cure induced residual stress in fiber direction. For all pre-cure levels examined, temperature overshoot was prevented from occurring both at the middle and top. For 0.25, 0.32 and 0.5 pre-cure levels, the reduction in temperature is 14.46 ^{o}C 15.28 ^{o}C and 16.09 ^{o}C respectively, at the middle compared to MRCC. At the top this reduction further increases and reaches 20.82 ^{o}C 21.30 ^{o}C and 22.71 ^{o}C for 0.25, 0.32 and 0.5 pre-cure levels, respectively.

Level of pre-cure	**Temperature Overshoot/ Undershoot (°C)**	**Reduction in °C**	**Stress at the end of dwell (MPa)**	**Stress Reduction in MPa / %**
1- MRCC	10,38	-	5,77	-
2- 0.25	-4.08	14.46	5.45	0,32 / 5.6%
3- 0.32	-4.90	15.28	5.53	0,24 / 4.2%
4- 0.5	-5.71	16.09	5.49	0,28 / 4.9%

Table 4.5: Temperature and cure induced residual stress results for different level of pre-cures at the middle (Model 3.2)

Level of pre-cure	**Temperature Overshoot/ Undershoot (°C)**	**Reduction in °C**	**Stress at the end of dwell (MPa)**	**Stress Reduction in MPa / %**
1- MRCC	10,38	-	5.42	-
2- 0.25	-10.44	20.82	4.98	0,44 / 8.1%
3- 0.32	-10.92	21.30	5.01	0,31 / 7.6%
4- 0.5	-12.33	22.71	5,20	0,22 / 4.1%

Table 4.6: Temperature and cure induced residual stress results for different level of pre-cures at the top (Model 3.2)

However, even though there is a reduction in the peak temperature reached, the stress values reached at the end are higher than the zero level of pre-cure, and as the level of pre-cure increases, stresses tend to increase. The reason for the increase in the stresses despite there being a decrease in the peak temperature is sub-laminates in this type of manufacturing are subjected to three different cure cycles while the previous case has two cure cycles. The gain obtained from the reduced peak temperature cannot compensate for the stress gained in the additional cure cycle. This leads to an increase in residual stresses.

4.3 Effect of Process Parameters on Cure and Residual Stress Formation

Due to the natural convection implemented at the top surface, the top region of the material ends up at a 0.87 degree of cure at the end when the MRCC is applied. In this section, the effect of several process parameters will be investigated to improve the level of final degree of cure, i.e. defined as a degree of minimally 0.9 and how these affect the cure-induced stresses. Four different variables are examined in the study: 1. convection coefficient, 2. two dwell cycle, 3. cure temperature, and 4. longer cure time.

The convection coefficient of 8 W/m^2K used in the models described before, contributes to the relatively low temperature at the top of the laminates during cure (55^oC). When the convection coefficient is lowered (more insulating), the temperature at equilibrium increases. This increases the degree of cure by about 0.05 in case of complete insulation. However, since the aim is to reach 0.9 at the top (being the region with the lowest degree of cure), the value of 4.8 W/m^2K is selected.

Second variable is the dwell temperature. Increasing dwell temperature is a direct method of increasing the temperature inside the material. Instead of using 70 ^0C dwell temperature, 80 ^0C is used. Thirdly, a longer dwell duration is examined. This is a selection that increases the manufacturing cost but since it does not increase the temperature overshoot or dwell temperature, its effect is also observed. Lastly, the effect of adding second dwell is investigated. The MRCC recommends a dwell duration of 4 hours at 70 ^oC degrees. A two-dwell cure cycle is designed to have 3 hours at 70 ^oC and 1 hour at 84 ^oC to reach the 0.9 degree of cure.

In figure 4.10 cure cycle applied for different conditions can be seen.

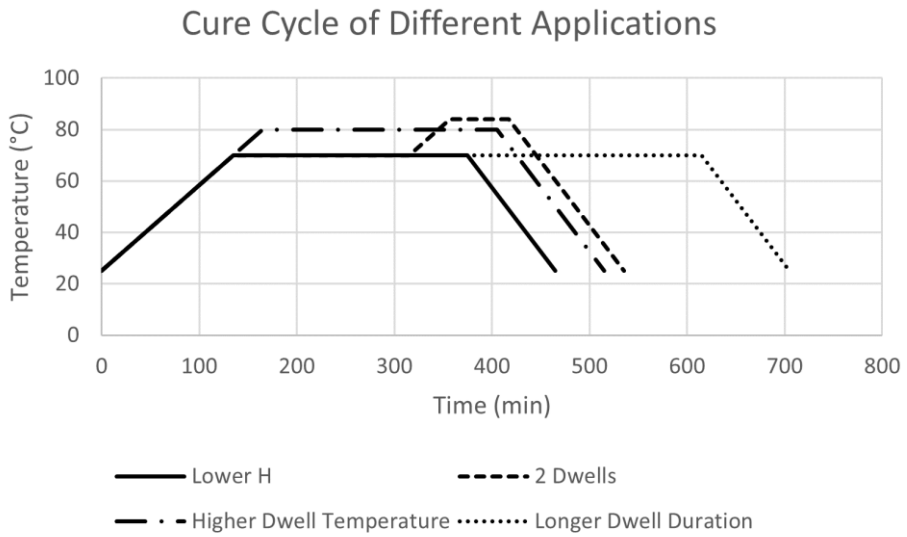

Figure 4.10: Different cure cycles applied to increase degree of cure

The results are presented for the top surface. As a result of these cure cycles application, temperature overshoot/undershoot values reached can be seen in Table 4.7. For the longer dwell duration case, the undershoot did not change (compared to MRCC) while for the other two cases it increased which are lower H and higher temperature. For the case which adds a second dwell, the temperature increased to 84 ^{o}C for 1 hour, but the second peak due to increased dwell temperature does not create a higher peak than the first one.

Process Parameter	**Temperature Overshoot/ Undershoot (°C)**	**Stress at the end of cool down (MPa)**
1- Lower H	1.31	13.15
2- Higher Temp.	-1.40	13.20
3- Longer Dwell	-5.09	13.65
4- Two Dwell	-5.09	13.00

Table 4.7: Temperature overshoot/undershoot at the top, and cure induced residual stress results for different process parameters

In this case, the stresses at the end of the cool down are presented since the cooldown starts at different temperatures for each case. As a result, adding second dwell generates less residual stresses 1.2% to 5% compared to the other cases considered. As a result of this analysis, it is observed that adding a second dwell after first dwell is the most beneficial one. The reason for that is, when second dwell starts, most of the chemical reaction is completed and once the temperature increased, the reaction to be completed does not contribute significantly to the temperature overshoot.

In literature, it is also found that lower ramp rates decrease temperature overshoot [83-84]. A similar study has been done to verify the literature. As a benchmark, Model 2 has been used. While comparing the effect of ramp rate, 0.33 ^{o}C/min is selected as a benchmark since all previous analysis have been done with 0.33 ^{o}C/min ramp rate. Table 4.8 shows the result of the study done at the middle section.

Ramp Rate	**Temperature Overshoot/ Undershoot (°C)**	**Reduction in °C**	**Stress at the end of cool down (MPa)**	**Stress Reduction in MPa / %**
1- 0.25	-1.80	1.02	5.19	0.25 / 4.6%
2- 0.33	-0.78	-	5.44	-
3- 0.50	4.47	-5.25	5.54	-0.10 / -1.8%

Table 4.8: Temperature overshoot/undershoot, and cure induced residual stress results for different ramp rates

As ramp rate decreases, reaction takes place in a longer time which allows it to dissipate the energy generated due to exotherm. It results in a lower value of temperature peak. Among three different ramp rates, the lowest one with 0.25^{o}C/min is the only one that can prevent temperature overshoot to occur.

As it was shown that adding a second dwell is a best way to increase the final degree of cure, the ramp rate and two dwells cure cycle were combined in a cure cycle. The selected ramp rate is 0.25 ^{o}C/min and first and second dwell temperatures are 50^{o}C and 70^{o}C, respectively. As a benchmark Model 3.1 chosen with 0.5 level of pre-cure since it provides least cure induced residual stress in fiber direction.

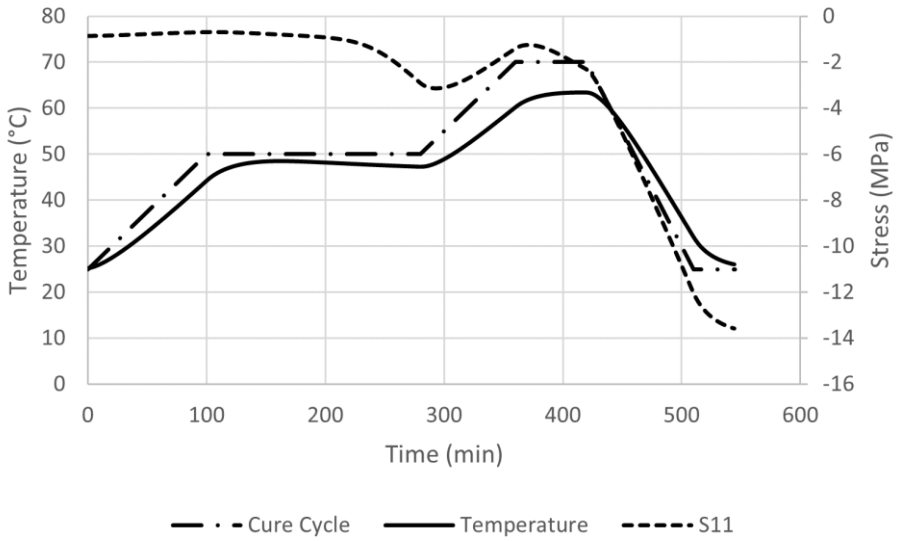

Figure 4.11: Result for low ramp rate, two-dwell cure cycle with 0.5 level of pre-cure at the middle (Model 3.1)

According to the evolution of longitudinal stress, see Figure 4.11, heating up the material with second dwell allows the material to build up tensile stresses. The reason for this is, during the second heating, process is expansion dominated and since it is after the gelation, modulus of resin is enough to develop tensile forces. This causes sort of relaxation of stresses that are already developed. This provides reduction from 5.52 MPa to 1.27 MPa in cure induced residual stresses in fiber direction before cool down that corresponds to 77% reduction and at the end of cool down reduction is from 15.9 MPa to 13.8 MPa that corresponds 13.2% compared to MRCC (i.e. Model 1). The gain loss at the end of the cool down is due to the fact that the effective cool down in the tailored cure cycle at the middle location is about 0.35 ^{o}C /min whilst when MRCC is applied the effective cool down seen at the middle location is 0.30 ^{o}C /min. Therefore, cool down will have to be optimized to keep the benefits.

5 Conclusion and future works

In this project, a coupled thermo-mechanical model is used to analyze the benefits introduced in terms of residual stresses generation when additive VARTM process is implemented. The thermo-mechanical model successfully calculates residual stress development for Airstone 780E/785H resin system and non-crimp biaxial E-glass fibers fabric by SAERTEX (812 g/m^2). Material properties develop during the cure cycle with a dependence on temperature and degree of cure. Although, the aim of the study is on different manufacturing methods, important results related to the resin system is obtained related to gelation, vitrification, and development of modulus.

This project shows that the additive VARTM process for manufacturing thick components is a way of decreasing the temperature overshoot and reducing the stresses developed at the end of the cure cycle. The benefit gained from the additive process is increasing as the thickness of the component increases. It is found that the most beneficial method is the additive VARTM process by using pre-cured sub-laminates (i.e. Model 3.1) provides 4.3% reduction in fiber direction stress compared to MRCC when a 31.5 mm thick component is considered. In case of 94.5 mm thick component, the reduction in fiber direction increases to 31.7%. The level of pre-cure is an important variable that affects the temperature overshoot and residual stress generation. As the level of pre-cure increases, the reduction in temperature overshoot and cure induced residual stress generation increases. Additional 7.8% reduction in cure induced residual stress in fiber direction can be obtained by increasing level of pre-cure up to 0.5 compared to MRCC. A tailored cure cycle with a ramp rate (of 0.25^{o}C/min), two-dwell temperature (i.e. 50 ^{o}C and 70 ^{o}C) and 0.5 level of pre-cure is suggested as well to show the potential of the additive process. Since the main aim of this project is not optimization of the cure cycle for thick components, the suggestion is based on literature research and results obtained. The aforementioned tailored cure cycle for additive VARTM process provides highest reduction in cure induced residual stresses in fiber direction by 76% (from 5.52 MPa down to 1.27 MPa) before cool down starts and 13.2% (from 15.9 MPa to 13.8 MPa) at the end of cool down compared to MRCC when 31.5 mm component is considered.

In future work, verification of the model can be accomplished by the manufacturing of suggested manufacturing methods with different pre-cure levels and measuring of temperature and residual strains by means of suitable sensors and by measuring warpage deformation. Also, an optimization study can be done to unleash the possible potential of the additive VARTM process. The thickness of the component may require ad-hoc cure cycles since it affects the amount of heat that is going to contribute to temperature overshoot.

References

[1] Park K.Y., Choi J.H. & Lee D.G., 1995. Delamination-free and high efficiency drilling of carbon fiber reinforced plastics. Journal of Composite Materials, 29(15), pp.1988–2002.

[2] 2022. Retrieved 2 August 2022, from https://www.compositesworld.com/cdn/cms/HPC-0902-A380feature-DaleBrosius.pdf

[3] Skordos A. & Kratz J., 2018. Layer by layer curing (LbL) Feasibility study final report.

[4] Yousefi A., Lafleur P.G. & Gauvin R., 1997. Kinetic studies of Thermoset Cure Reactions: A Review. Polymer Composites, 18(2), pp.157–168.[5] Sozer E.M., Simacek P. & Advani S.G., 2012. Resin transfer molding (RTM) in Polymer Matrix Composites. Manufacturing Techniques for Polymer Matrix Composites (PMCs), pp.245–309.

[6] Kuentzer N., Simacek P., Advani S., Walsh S., 2007. Correlation of Void Distribution to VARTM manufacturing techniques. Composites Part A: Applied Science and Manufacturing, 38(3), pp.802–813.

[7] Song X., 2003. Vacuum Assisted Resin Transfer Molding (VARTM): Model Development and Verification. PhD Thesis, Virginia Polytechnic Institute and State University.

[8] Tamakuwala V., 2021. Manufacturing of fiber reinforced polymer by using VARTM process: A review. Materials Today: Proceedings, 44, p.p. 987-993.

[9] Nielsen M., 2013. Prediction of process induced shape distortions and residual stresses in large fibre reinforced composite laminates: With application to Wind Turbine Blades. PhD Thesis, TU Denmark.

[10] Shah D. & Schubel P. 2010. Evaluation of cure shrinkage measurement techniques for thermosetting resins. Polymer Testing, 29(6), p.p. 629-639.

[11] Peng W. & Riedl B., 1995. Thermosetting Resins. Journal Of Chemical Education, 72(7), 587.

[12] Heise M., Martin G. & Gotro J., 1990. Gelation in thermosets formed by chain addition polymerization. Polymer Engineering And Science, 30(2), p.p. 83-89.

[13] Khoun L., Centea T. & Hubert P., 2010. Characterization methodology of thermoset resins for the processing of composite materials - case study: CYCOM 890RTM epoxy resin. Journal of Composite Materials, 44(11): p.p. 1397–1415.

[14] Yousefi A., Lafleur P.G. & Gauvin R., 1997. Kinetic studies of Thermoset Cure Reactions: A Review. Polymer Composites, 18(2), pp.157–168.

[15] Kissinger H.E., 1957. Reaction kinetics in differential thermal analysis. Analytical Chemistry, 29(11), pp.1702–1706.

[16] SHI. L., 2016. Heat Transfer in the Thick Thermoset Composites. Phd thesis, Northwestern Polytechnical University

[17] Kamal M.R., 1974. Thermoset characterization for Moldability analysis. Polymer Engineering and Science, 14(3), pp.231–239.
[18] Bogetti T.A. & Gillespie J.W., 1992. Process-induced stress and deformation in thick-section thermoset composite laminates. Journal of Composite Materials, 26(5), pp.626–660.
[19] Griffin O.H., 1983. Three-dimensional curing stresses in symmetric cross-ply laminates with temperature-dependent properties. Journal of Composite Materials, 17(5), pp.449–463.
[20] Zarrelli M., Partridge I.K. & D'Amore A., 2006. Warpage induced in bi-material specimens: Coefficient of thermal expansion, chemical shrinkage and viscoelastic modulus evolution during cure. Composites Part A: Applied Science and Manufacturing, 37(4), pp.565–570.
[21] Abou Msallem Y., Jacquemin F., Boyard N. Poitou, A., et al., 2010. Material characterization and residual stresses simulation during the manufacturing process of epoxy matrix composites. Composites Part A: Applied Science and Manufacturing, 41(1), pp.108–115.
[22] Blanco S., You H., Kerekes T. & Yun G., 2021. Cure-induced residual stress buildup and distortions of CFRP laminates with Stochastic Thermo-Chemical and viscoelastic models: Experimental verifications. Mechanics of Advanced Materials and Structures, 29(19), pp.2740–2756.
[23] Lee S. M., & Schile R. D. 1982. An investigation of material variables of epoxy resins controlling transverse cracking in composites. Journal of Materials Science, 17(7), p.p. 2095–2106.
[24] Bogetti T. A. & Gillespie J.W. Jr., 1991. Two-Dimensional Cure Simulation of Thick Thermosetting Composites, Journal of Composite Materials, 25(3): p.p. 239-273
[25] Bateman M. G., Miller O. H., Palmer T. J., Breen C.E.P., et al., M. J. 2005. Measurement of residual stress in thick section composite laminates using the deep-hole method. International Journal of Mechanical Sciences, 47(11), p.p. 1718–1739.
[26] Oh J.H. & Lee D.G., 2002. Cure cycle for thick glass/epoxy composite laminates. Journal of Composite Materials, 36(1), pp.19–45.
[27] Hojjati M. & Hoa S., 1994. Curing simulation of thick thermosetting composites, Composites Manufacturing, vol. 5, no. 3, pp. 159–169.
[28] Kravchenko O.G., Kravchenko S.G., & Pipes R.B., 2019. Cure history dependence of residual deformation in a thermosetting laminate, Composites Part A: Applied Science and Manufacturing, vol. 99, pp. 186–197.
[29] Kim K.S. & Hahn H.T., 1989. Residual stress development during processing of graphite/epoxy composites. Composites Science and Technology, 36(2), pp.121–132.
[30] Harper B. & Weitsman Y., 1981. Residual thermal stresses in an unsymmetrical cross-ply graphite/epoxy laminate. 22nd Structures, Structural Dynamics and Materials Conference.
[31] Zarrelli M., 2003. Cure induced property changes and warpage in thermoset resins and composites. PhD thesis, Cranfield University.

[32] Zarrelli, M., Skordos, A.A. & Partridge, I.K., 2002. Investigation of CURE induced shrinkage in unreinforced epoxy resin. Plastics, Rubber and Composites, 31(9), pp.377–384.
[33] Yoon K.J. & Kim J.S., 2001. Effect of thermal deformation and chemical shrinkage on the process induced distortion of carbon/epoxy curved laminates. Journal of Composite Materials, 35(3), pp.253–263.
[34] Hodges J., Yates B., Darby M. I., Wostenholm, G. H., et al., T. F. 1989. Residual stresses and the optimum cure cycle for an epoxy resin. Journal of Materials Science, 24(6), p.p. 1984–1990.
[35] Gopal A.K., Adali S. & Verijenko V.E., 2000. Optimal temperature profiles for minimum residual stress in the cure process of polymer composites. Composite Structures, 48(1-3), pp.99–106
[36] Dolkun D., Zhu W., Xu Q. & Ke Y., 2018. Optimization of CURE profile for thick composite parts based on finite element analysis and genetic algorithm. Journal of Composite Materials, 52(28), pp.3885–3894.
[37] Dong A., Zhao Y., Zhao X. & Yu Q., 2018. Cure cycle optimization of rapidly cured out-of-autoclave composites. Materials, 11(3), p.421.
[38] Kumar A. A., & Sundaram R., 2016. Cure cycle optimization for the resin infusion technique using carbon nanotube additives. Carbon, 96, p.p. 1043-1052.
[39] Khattab A., 2013. Cure cycle effect on high-temperature polymer composite structures molded by Vartm. Journal of Composites, 2013, pp.1–6.
[40] Kravchenko O.G., Kravchenko S.G. & Pipes, R.B., 2016. Chemical and thermal shrinkage in thermosetting prepreg. Composites Part A: Applied Science and Manufacturing, 80, pp.72–81.
[41] Lange J., Toll S., Manson J. & Hult A., 1997. Residual stress build-up in thermoset films cured below their ultimate glass transition temperature. Polymer, 38(4), pp.809–815.
[42] Khoun L. & Hubert P., 2010. Investigation of the dimensional stability of carbon epoxy cylinders manufactured by resin transfer moulding. Composites Part A: Applied Science and Manufacturing, 41(1), pp.116–124.
[43] Bowles D., & Tompkins S., 1989. Prediction of Coefficients of Thermal Expansion for Unidirectional Composites. Journal Of Composite Materials, 23(4), p.p. 370-388.
[44] Wisnom M.R., Gigliotti M., Ersoy N., Campbell M., et al., 2006. Mechanisms generating residual stresses and distortion during manufacture of polymer–matrix composite structures. Composites Part A: Applied Science and Manufacturing, 37(4), pp.522–529.
[45] Ishikawa T. & Chou T.-W., 1983. In-plane thermal expansion and thermal bending coefficients of fabric composites. Journal of Composite Materials, 17(2), pp.92–104.
[46] Fletcher A.J. & Oakeshott J.L., 1994. Thermal residual microstress generation during the processing of unidirectional carbon fibre/epoxy resin composites: Random fibre arrays. Composites, 25(8), pp.806–813.

[47] Parlevliet P.P., Bersee H.E.N. & Beukers, A., 2007. Residual stresses in thermoplastic composites – a study of the literature. part III: Effects of thermal residual stresses. Composites Part A: Applied Science and Manufacturing, 38(6), pp.1581–1596.
[48] Nakamura T. & Suresh S., 1993. Effects of thermal residual stresses and fiber packing on deformation of metal-matrix composites. Acta Metallurgica et Materialia, 41(6), pp.1665–1681.
[49] Hu G.K. & Weng G.J., 1998. Influence of thermal residual stresses on the composite macroscopic behavior. Mechanics of Materials, 27(4), pp.229–240
[50] Hyer M.W., 1981. Some observations on the cured shape of thin unsymmetric laminates. Journal of Composite Materials, 15(2), pp.175–194.
[51] Melo J.D., Radford D.W., 1999. Modeling manufacturing distortions in flat symmetric, composite laminates. In: 31st International SAMPE Technical Conference. p. 592–603
[52] Radford D.W., Fu S., Derringer D., & Davis J.D., 1999. Measurement of manufacturing distortion in flat composite laminates. In 12th International Conference on Composite Materials.
[53] Zarrelli M., Skordos A.A. & Partridge I.K., 2002. Investigation of CURE induced shrinkage in unreinforced epoxy resin. Plastics, Rubber and Composites, 31(9), pp.377–384.
[54] Nawab Y., Shahid S., Boyard N.& Jacquemin F., 2013. Chemical shrinkage characterization techniques for thermoset resins and associated composites. Journal of Materials Science, 48(16), pp.5387–5409.
[55] Hu H., Li S., Wang J., Zu L., et al., 2017. Monitoring the gelation and effective chemical shrinkage of composite curing process with a novel FBG approach. Composite Structures, 176, pp.187–194.
[56] Abouhamzeh M., Sinke J., Jansen K., & Benedictus, R., 2015. Closed form expression for residual stresses and warpage during cure of composite laminates. Composite Structures, 133, p.p. 902-910.
[57] Hahn H.T. & Pagano N.J., 1975. Curing stresses in composite laminates. Journal of Composite Materials, 9(1), pp.91–106.
[58] Potter K., Campbell M., Langer C. & Wisnom M., 2005. The generation of geometrical deformations due to tool/part interaction in the manufacture of composite components. Composites Part A: Applied Science and Manufacturing, 36(2), pp.301–308.
[59] Twigg G., Poursartip A. & Fernlund G., 2004. Tool–part interaction in composites processing. part II: Numerical modelling. Composites Part A: Applied Science and Manufacturing, 35(1), pp.135–141.
[60] Twigg G., 2003. An experimental method for quantifying tool–part shear interaction during composites processing. Composites Science and Technology, 63(13), pp.1985–2002.
[61] Li Y., Xiao Y., Yu L., Ji K., et al., 2022. A review on the tooling technologies for composites manufacturing of aerospace structures: Materials, structures and Processes. Composites Part A: Applied Science and Manufacturing, 154, p.106762.

[62] White S., & Hahn H. 1992. Process Modeling of Composite Materials: Residual Stress Development during Cure. Part I. Model Formulation. Journal Of Composite Materials, 26(16), p.p. 2402-2422.
[63] Kamal M.R., 1974. Thermoset characterization for Moldability analysis. Polymer Engineering and Science, 14(3), pp.231–239.
[64] Struzziero G., & Teuwen J., 2019. Effect of convection coefficient and thickness on optimal cure cycles for the manufacturing of wind turbine components using VARTM. Composites Part A: Applied Science And Manufacturing, 123, p.p. 25-36.
[65] Guo Z.S, Du S. & Zhang B., 2005. Temperature field of thick thermoset composite laminates during cure process, Composite Science and Technology, vol. 65, pp. 517-523.
[66] Bogetti T.A., John H. & Gillespie J.W., 1991. Two-Dimensional Cure Simulation of Thick Thermosetting Composites, Journal of Composite Materials, vol. 25.
[67] Cheung A., Yu Y. & Pochiraju K., 2004. Three-dimensional finite element simulation of curing of polymer composites, Finite Element in Analysis and Design, vol. 40, pp. 895-912.
[68] Loon T.M.J.v., 2016. Influence of ply drop-off regions on the cure-induced residual stress development within thermoset composites manufactured by resin transfer moulding, MSc thesis, TU Delft.
[69] ABAQUS User Subroutines Reference Manual (v6.6). 2022.
[70] Hubert P., Johnston A.A., Poursartip A. & Nelson K., 2001. Cure Kinetics and Viscosity Models for Hexcel 8552 Epoxy Resin, p.p. 2341–2354.
[71] Skordos AA & Partridge IK. Inverse heat transfer for optimization and on-line thermal properties estimation in composites curing, p.p. 157–72.
[72] Farmer J. & Covert E., 1996. Thermal conductivity of a thermosetting advanced composite during its cure, p.p. 467–75.
[73] Yamane T., Katayama S., Todoki M. & Hatta I., 2000. The measurements of thermal conductivity of carbon fibers, p.p. 294–305.
[74] Schapery R.A., 1968. Thermal Expansion Coefficients of Composite Materials Based on Energy Principles. Journal of Composite Materials, 2(3): p.p. 380–404,.
[75] Struzziero G., Nardi D., Sinke J. & Teuwen J. 2020. Cure-induced residual stresses for warpage reduction in thermoset laminates. Journal Of Composite Materials, 54(22), p.p. 3055-3065.
[76] Chamis C.C., 1989. Mechanics of composite materials: Past, present, and future. Journal of Composites Technology and Research, 11(1): p.p. 3–14.
[77] Skrzypek J. & Ganczarski A., 2015. *Mechanics of Anisotropic Materials*.
[78] Khoun L., Centea T. & Hubert P., 2010. Characterization methodology of thermoset resins for the processing of composite materials - case study: CYCOM 890RTM epoxy resin. Journal of Composite Materials, 44(11): p.p. 1397–1415.

[79] Chava S., & Namilae S., 2021. Continuous evolution of processing induced residual stresses in composites: An in-situ approach. Composites Part A: Applied Science And Manufacturing, 145, 106368.
[80] Struzziero G., & Teuwen J., 2020. A fully coupled thermo-mechanical analysis for the minimisation of spring-in and process time in ultra-thick components for wind turbine blades. Composites Part A: Applied Science And Manufacturing, 139, 106105.
[81] Shah P.H., Halls V.A., Zheng J.Q. & Batra R.C., 2017. Optimal cure cycle parameters for minimizing residual stresses in fiber-reinforced polymer composite laminates. Journal of Composite Materials, ;52(6): p.p. 773-92
[82] White S.R. & Hahn H.T., 1993. Cure cycle optimization for the reduction of processing-induced residual stresses in composite materials. Journal of Composite Materials.;27(14): p.p. 1352-78.
[83] Struzziero G. & Skordos A. A. 2017. Multi-objective optimisation of the cure of thick components. Composites Part A: Applied Science and Manufacturing, 93, p.p. 126–136.
[84] Li M., Zhu Q., Geubelle P.H. & Tucker III C.L., 2001. Optimal curing for thermoset matrix composites: thermochemical considerations. Polymer Compos ;22 (1): p.p. 118–31.
[85] AirstoneTM Infusion System Product, (accessed 17 May 2022). www.olinepoxy.com
[86] Tavakol B., Roozbehjavan P., Ahmed A., Das R., et al., 2012. Prediction of residual stresses and distortion in carbon fiber-epoxy composite parts due to curing process using finite element analysis. Journal of Applied Polymer Science, 128(2), pp.941–950.

A User-Subroutine

```
      SUBROUTINE SDVINI(STATEV,COORDS,NSTATV,NCRDS,NOEL,NPT,
     1 LAYER,KSPT)
C
      INCLUDE 'ABA_PARAM.INC'
C
      DIMENSION STATEV(NSTATV),COORDS(NCRDS)

      DOUBLE PRECISION DOC_initial

      DOC_initial=8.0D-2              !Set initial DOC
      STATEV(20)=DOC_initial
      RETURN
      END

      SUBROUTINE UMAT(STRESS,STATEV,DDSDDE,SSE,SPD,SCD,
     1 RPL,DDSDDT,DRPLDE,DRPLDT,
     2 STRAN,DSTRAN,TIME,DTIME,TEMP,DTEMP,PREDEF,DPRED,CMNAME,
     3 NDI,NSHR,NTENS,NSTATV,PROPS,NPROPS,COORDS,DROT,PNEWDT,
     4 CELENT,DFGRD0,DFGRD1,NOEL,NPT,LAYER,KSPT,JSTEP,KINC)
      INCLUDE 'ABA_PARAM.INC'
C
      CHARACTER*80 CMNAME

      DIMENSION STRESS(NTENS),STATEV(NSTATV),
     1 DDSDDE(NTENS,NTENS),DDSDDT(NTENS),DRPLDE(NTENS),
     2 STRAN(NTENS),DSTRAN(NTENS),TIME(2),PREDEF(1),DPRED(1),
     3 PROPS(NPROPS),COORDS(3),DROT(3,3),DFGRD0(3,3),DFGRD1(3,3),
     4 JSTEP(4)

      DIMENSION ELASSTRAN(NTENS),DTHERMSTRAN(NTENS),THERMSTRAN(NTENS),
     1 CHEMSTRAN(NTENS),DCHEMSTRAN(NTENS)

      DOUBLE PRECISION DOC_max,v_f,DOC,A,E,n,m,C,alpha_c,alpha_T,H_tot,
     1 R,rho_f,rho_r,rho_laminate,E_lf,E_tf,G12_f,G23_f,NU12_f,a_lf,
     2 a_tf,E_r_glass,E_r_glassT,E_r_rub,NU_r_glass,NU_r_rub,a_glass,
     3 a_rub,y_a,Cm,sigma_m,Tg_0,Tg_inf,LAMBDA,DOC_old,CureRate,Tg,
     4 E_r,NU_r,G_r,a_r,y_r,E1,E2,E3,G12,G13,G23,NU_12,NU_13,NU_23,
     5 NU_21,NU_31,NU_32,DELTA,a_l,a_t,y_l,y_t,DOC_initial,TEMP_initial
      INTEGER I,J

      PARAMETER (ZERO=0.0D0, ONE=1.0D0, TWO=2.0D0)

C================================Manual input of DOC_max and laminate v_f==========================!
C     DOC_initial=8.0D-2          !Set initial DOC
      DOC_max = 0.9999                    !Set maximum DOC
      v_f=0.54                            !Assumed fibre volume fraction of the laminate
C ============================Obtaining state variables 1-19 from previous increment=====================!
      DO I=1,NTENS
       ELASSTRAN(I) = STATEV(I)
       THERMSTRAN(I) = STATEV(I+NTENS)
```

```
      CHEMSTRAN(I) = STATEV(I+TWO*NTENS)
      ENDDO

      DOC=STATEV(20)

C           Cure kinetic parameters, based on Airstone 780E/785H resin (obtained from Struzziero2019a)
      A=681085.0              !Pre-exponential Arrhenius factor [s^-1]
      E=59291.0               !Activation energy [J/mol^-1]
      n=1.67                  !Reaction order [-]
      m=0.12                  !Reaction order [-]
      C=47.7                  ![-]
      alpha_c=0.77            ![-]
      alpha_T=1.60D-3         ![degC^-1]
      H_tot=434.0D3           ![J*kg^-1]
      R=8.3145                !Universal gas constant [J K^â^'1 mol^â^'1]

C ================================Material parameters of constituents=================================!
            !---Glass fibre---!
            !Mechanical
      E_lf=73.1D9             !Young's modulus glass fibre longitudinal direction [Pa] (Struzziero2020)
      E_tf=73.1D9             !Young's modulus glass fibre transverse direction [Pa] (Struzziero2020)
      G12_f=30.0D9            !Shear modulus fibre 12-direction [Pa] (Struzziero2020)
      G23_f=30.0D9            !Shear modulus fibre 23-direction [Pa] (same as G12_f since glass fibre is isotropic)
      NU12_f=0.22             !Poisson's ratio of fibre in 12-direction [-] (Struzziero2020)
            !Thermal
      a_lf=5.0D-6             !CTE in longitudinal direction [1/degC]
      a_tf=5.0D-6             !CTE in transverse direction [1/degC]

            !---Epoxy resin---!
            !Mechanical
      E_r_glass=4.61D9        !Modulus resin at glassy state [Pa] (Struzziero2020)
      E_r_glassT=-0.012D9     !Temperature depence of modulus at glassy state [Pa/degC] (Struzziero2020)
      E_r_rub=0.04D9          !Modulus resin at rubbery state [Pa] (Struzziero2020)
      NU_r_glass=0.35         !Poisson's ratio resin at glassy state [-] (Obrien2001)
      NU_r_rub=0.49999        !Poisson's ratio resin at rubbery state [-] (Obrien2001)

            !Thermal expansion
      a_glass=6.0D-5          !CTE resin at glassy state [1/degC] (Struzziero2020)
      a_rub=1.7D-4            !CTE resin at rubbery state [1/degC] (Struzziero2020)

            !Chemical linear strain due to shrinkage
      y_a=1.9D-2              !Linear shrinkage of resin [-] (Struzziero2020)

      !Others
      Cm=0.4                  !Breadth of transition [1/degC] (Struzziero2020)
      sigma_m=10.2            !Temperature shift of transition [degC] (Struzziero2020)

            !Glass transition temperature parameters
      Tg_0=-55.0              !Minimum Tg of epoxy resin [degC] (Struzziero2019a)
      Tg_inf=89.0             !Maximum Tg of epoxy resin [degC] (Struzziero2019a)
      LAMBDA=0.476            !Fitting parameter [-](Struzziero2019a)
```

```
            !Evolution of Glass transition temperature (DiBenedetto Eq.)
      Tg=Tg_0+((Tg_inf-Tg_0)*LAMBDA*DOC)/(1-(1-LAMBDA)*DOC)

            !Mechanical property evolutions throughout cure development
      E_r= E_r_rub + (E_r_glass+(E_r_glassT*TEMP)-E_r_rub)/
     &           (1+exp(Cm*(TEMP-Tg-sigma_m)))                    !Transition of resin modulus [MPa]
      NU_r=NU_r_rub + (NU_r_glass-NU_r_rub)/
     &           (1+exp(Cm*(TEMP-Tg-sigma_m)))                    !Transition of resin Poisson's ratio [-]
      G_r=E_r/(2*(1+NU_r))                                                    !Resin shear modulus
[MPa]


C ==============Property calculation of composite (transversely isotropic)======================!
            !-----------Mechanical (transversely isotropic)------!
      E1=v_f*E_lf + (1-v_f)*E_r                !Young's modulus in 1-direction [Pa] (Chamis1989)
      E2=E_r/(1-sqrt(v_f)*(1-(E_r/E_tf)))      !Young's modulus in 2-direction [Pa] (Chamis1989)
      E3=E2                                                    !Young's modulus in 3-direction [Pa] (Chamis1989)

      G12=G_r/(1-sqrt(v_f)*(1-(G_r/G12_f)))   !Shear modulus in 12-direction [Pa] (Chamis1989)
      G13=G12                                                  !Shear modulus in 13-direction [Pa] (Chamis1989)
      G23=G_r/(1-sqrt(v_f)*(1-(G_r/G23_f)))   !Shear modulus in 13-direction [Pa] (Chamis1989)

      NU_12=v_f*NU12_f + (1-v_f)*NU_r          !Poisson's ratio in 12-direction [-] (Chamis1989)
      NU_13=NU_12                                              !Poisson's ratio in 13-direction [-] (Chamis1989)
      NU_23=(E2/(2*G23))-1                                     !Poisson's ratio in 23-direction [-] (Chamis1989)

      NU_21=(E2/E1)*NU_12                                      !Poisson's ratio in 21-direction [-] (Stress tensor symmetry)
      NU_31=(E3/E1)*NU_13                                      !Poisson's ratio in 31-direction [-] (Stress tensor symmetry)
      NU_32=(E3/E2)*NU_23                                      !Poisson's ratio in 32-direction [-] (Stress tensor symmetry)

      DELTA=ONE-NU_12*NU_21-NU_13*NU_31-NU_23*NU_32
     &       -NU_12*NU_23*NU_31-NU_21*NU_32*NU_13

C =========================Resin material parameters evolution models====================================!
            !Calculation of the curing rate with autocatalytic kinetic model (with T in kelvin)
      CureRate = (A*exp(-E/(R*(TEMP+273.15))))/
     &         (1+exp(C*(DOC-alpha_c-alpha_T*(TEMP))))
     &         *(1-DOC)**n * DOC**m
      !Calculation of new DOC
      DOC_new = DOC + CureRate*DTIME
C     WRITE(6,*) 'DTIME is: ' DTIME

            !When new DOC is exceeding DOC_max, this DOC value is used and CureRate is terminated
      IF (DOC_new .gt. DOC_max) THEN
        DOC_new = DOC_max
        CureRate=0.0
      END IF

            !Thermal expansion evolutions throughout cure development [1/degC]
      a_r=a_rub + (a_glass - a_rub)/(1+exp(Cm*(TEMP-Tg-sigma_m)))

            !Incremental Chemical shrinkage of the resin due to DOC development
      y_r=y_a*(DOC_new-DOC)
```

```
      !----------------Thermal expansion--------------!
a_l=(((1-v_f)*E_r*a_r) + v_f*E_lf*a_lf)/((1-v_f)*E_r + v_f*E_lf)  !Thermal expansion in 1-direction [1/degC]
a_t=(1-v_f)*a_r + v_f*a_tf + (1-v_f)*a_r*NU_r
&          + NU12_f*a_lf*v_f-NU_12*a_l                    !Thermal expansion in 2/3-direction [1/degC]

      !---------------Chemical shrinkage--------------!
y_l=(((1-v_f)*E_r*y_r)) /((1-v_f)*E_r + v_f*E_lf)          !Chemical shrinkage in 1-direction [-]
y_t=(1-v_f)*y_r + (1-v_f)*y_r*NU_r - NU12_f*y_l                  !Chemical shrinkage in 2/3-direction [-]

      !Create empty stiffness matrix
DO I=1,NTENS
 DO J=1,NTENS
 DDSDDE(I,J)=ZERO
 ENDDO
ENDDO

      !The following lines define the 12 different entities of the stiffness matrix
      !for an transversely isotropic linear elastic material. (Mechanics of Anisotropic Materials, Skrzypek2015)
DDSDDE(1,1)=((ONE-NU_23*NU_32)/DELTA)*E1
DDSDDE(1,2)=((NU_12+NU_13*NU_32)/DELTA)*E2
DDSDDE(1,3)=((NU_13+NU_12*NU_23)/DELTA)*E3
DDSDDE(2,1)=DDSDDE(1,2)
DDSDDE(2,2)=((ONE-NU_13*NU_31)/DELTA)*E2
DDSDDE(2,3)=((NU_23+NU_21*NU_13)/DELTA)*E3
DDSDDE(3,1)=DDSDDE(1,3)
DDSDDE(3,2)=DDSDDE(2,3)
DDSDDE(3,3)=((ONE-NU_12*NU_21)/DELTA)*E3
DDSDDE(4,4)=G12
DDSDDE(5,5)=G13
DDSDDE(6,6)=G23

      !Define Thermal Strain tensor for this increment
DTHERMSTRAN(1)=a_l*DTEMP
DTHERMSTRAN(2)=a_t*DTEMP
DTHERMSTRAN(3)=DTHERMSTRAN(2)
DO J=NDI+1,NTENS
 DTHERMSTRAN(J)=ZERO
ENDDO

      !Define Incremental chemical strain tensor for this increment
DCHEMSTRAN(1)=-y_l
DCHEMSTRAN(2)=-y_t
DCHEMSTRAN(3)=DCHEMSTRAN(2)
DO J=NDI+1,NTENS
 DCHEMSTRAN(J)=ZERO
ENDDO

      !Define the new stress tensor by using the previous calculated stiffness entity with
      !the corresponding stress vector and strain vector entity.
DO I=1,NTENS
 DO J=1,NTENS
  STRESS(J)=STRESS(J)+DDSDDE(J,I)*(DSTRAN(I)-
```

```
     &          (DTHERMSTRAN(I)+DCHEMSTRAN(I)))
      ENDDO
            !Sum incremental elastic and thermal strains in total strain arrays
      ELASSTRAN(I) = ELASSTRAN(I) + (DSTRAN(I)-(DTHERMSTRAN(I)+DCHEMSTRAN(I)))
      THERMSTRAN(I) = THERMSTRAN(I) + DTHERMSTRAN(I)
      CHEMSTRAN(I) = CHEMSTRAN(I) + DCHEMSTRAN(I)
     ENDDO

            !Save Elastic, thermal and chemical strain for next increment.
     DO I=1,NTENS
      STATEV(I) = ELASSTRAN(I)
      STATEV(I+NTENS) = THERMSTRAN(I)
      STATEV(I+TWO*NTENS) = CHEMSTRAN(I)
     ENDDO

            !Save new DOC, CureRate,Tg for next increment
     STATEV(19)=DOC                  !Needed for current increment as DOC in UMATHT
     STATEV(20)=DOC_new              !Needed for next increment as DOC_old
     STATEV(21)=CureRate             !Needed to export for heat development in UMATHT
     STATEV(22)=Tg                   !Needed to export the Tg for equations in UMATHT
     STATEV(23)=E3
C    STATEV(24)=y_t
     RETURN
     END

     SUBROUTINE DISP(U,KSTEP,KINC,TIME,NODE,NOEL,JDOF,COORDS)

     INCLUDE 'ABA_PARAM.INC'
     COMMON  Tbound
     Common/convectio/T1,T2,Dt1,ra1,ra2,Dt2,r1,T0,r2,rc,rac,totaltime,
    &wt
     DIMENSION U(3),TIME(3),COORDS(3)
     DOUBLE PRECISION T0,T1,Dt1,r1,T2,Dt2,r2,rc,ra1,ra2,rac,totaltime,
    &wt
     real*8 Tbound
!================================Input variables=======================================!
     T0=25                   !Predefined Temperature (Must be equal to CAE model predefined Temp.)
            ! parameters
     T1=70                   !Temperature First dwell [degC]
     T2=70
     Dt1=14000                       !Duration of First dwell [s]

     r1=0.333333                     !Heating rate [degC/min]

     Dt2=400                 !Duration of Second dwell [s]
     r2=0.5                  !Heating rate [degC/min]
     rc=0.5                  !Cooling rate [degC/min]
     T4=25     !Temperature of the environment
!================================Parameter recalculation=======================================!
!    Recalculate heating rate to seconds
     r1=r1/60                        !Rate 1, [degC/s]
     r2=r2/60                        !Rate 2, [degC/s]
     rc=rc/60                        !Rate 3, [degC/s]
```

```
!    Recalculate Temp's and rates to time durations
     ra1=((T1-T0)/r1)
     ra2=(T2-T1)/r2
     rac=(T2-T0)/rc
     wt=0  !waiting time for the second cure cycle
     totaltime=ra2+Dt1+ra1+Dt2+rac+wt
!    Cure cycle definition
     IF (TIME(2)<=ra1+wt) THEN
      U(1)=T0+r1*(TIME(2)-wt)

     ELSE IF (TIME(2)>ra1+wt.and.TIME(2)<=ra1+Dt1+wt) THEN
      U(1)=T1

     ELSE IF (TIME(2)>ra1+Dt1+wt.and.TIME(2)<=ra2+Dt1+ra1+wt) THEN
      U(1)=T1 + r2*(TIME(2)-Dt1-ra1-wt)

     ELSE IF (TIME(2)>ra1+Dt1+ra2+wt.and.TIME(2)<=ra2+Dt1+ra1+Dt2+wt)
    & THEN
      U(1)=T2

     ELSE IF
    1 (TIME(2)>ra1+Dt1+Dt2+ra2+wt.and.TIME(2)<=ra2+Dt1+ra1+Dt2+rac+wt)
    2 THEN
      U(1)=T2- rc*(TIME(2)-Dt1-ra1-Dt2-ra2-wt)
     ELSE IF  (TIME(2)>=ra1+Dt1+ra2+Dt2+rac+wt) THEN
      U(1)=T0
     END IF
     Tbound=U(1)
     RETURN
     END

     SUBROUTINE FILM(H,SINK,TEMP,KSTEP,KINC,TIME,NOEL,NPT,
    1 COORDS,JLTYP,FIELD,NFIELD,SNAME,NODE,AREA)
C
     INCLUDE 'ABA_PARAM.INC'
     DIMENSION H(2),TIME(2),COORDS(3), FIELD(NFIELD)
     COMMON/param/Tbound,flag,amin,stinc,flag1,Tmax,amax,nmax
     COMMON/paramet/v,t
     Common/convectio/T1,T2,Dt1,ra1,ra2,Dt2,r1,T0,r2,rc,rac,totaltime
     CHARACTER*80 SNAME
     real*8 hnatur,sp,len
     hnatur=8
     H(1)=hnatur
     IF (TIME(2)<=ra1+wt) THEN
      sink=T0
     ELSE IF (TIME(2)>ra1+wt.and.TIME(2)<=ra1+Dt1+wt) THEN
      sink=T0
     ELSE IF (TIME(2)>ra1+Dt1+wt.and.TIME(2)<=ra2+Dt1+ra1+wt) THEN
      sink=T0
     ELSE IF (TIME(2)>ra1+Dt1+ra2+wt.and.TIME(2)<=ra2+Dt1+ra1+Dt2+wt)
    &  THEN
      sink=T0
     ELSE IF (TIME(2)>ra1+Dt1+Dt2+ra2+wt.and.TIME(2)<=totaltime) THEN
```

```
      sink=T0
      ELSE IF  (TIME(2)>=ra1+Dt1+ra2+Dt2+rac+wt) THEN
      sink=T0
     END IF
     RETURN
     END

     SUBROUTINE UMATHT(U,DUDT,DUDG,FLUX,DFDT,DFDG,
    1 STATEV,TEMP,DTEMP,DTEMDX,TIME,DTIME,PREDEF,DPRED,
    2 CMNAME,NTGRD,NSTATV,PROPS,NPROPS,COORDS,PNEWDT,
    3 NOEL,NPT,LAYER,KSPT,KSTEP,KINC)

     INCLUDE 'ABA_PARAM.INC'

     CHARACTER*80 CMNAME

     DIMENSION DUDG(NTGRD),FLUX(NTGRD),DFDT(NTGRD),
    1 DFDG(NTGRD,NTGRD),STATEV(NSTATV),DTEMDX(NTGRD),
    2 TIME(2),PREDEF(1),DPRED(1),PROPS(NPROPS),COORDS(3)

     DOUBLE PRECISION DOC,CureRate,Tg,H_tot,v_f,Q,K(NTGRD),K_lf,K_tf,
    1 a_kr,b_kr,c_kr,d_kr,e_kr,f_kr,K_r,K11,K22,K33,A_fcp,B_fcp,A_rcp
    2 B_rcp,delta_rcp,C_rcp,sigma,rho_f,rho_r,w_f,Cp_f,Cp_r,Cp_c
     PARAMETER (ZERO=0.0D0, ONE=1.0D0, TWO=2.0D0)

          !Initialize STATEV.
     DOC = STATEV(19)                    !Obtaining DOC from UMAT
     CureRate=STATEV(21)                 !Obtaining CureRate from UMAT
     Tg=STATEV(22)                       !Obtaining Tg from UMAT

     H_tot=434.0D3                       !Reaction energy [J*kg^-1]
     v_f=0.54                                  !Assumed fibre volume fraction of the laminate (must me same as in other
subroutines)

          !Heat generation source definition
     Q=(1-v_f)*H_tot*CureRate*DTIME*(1100/(0.54*2500+0.46*1100))
          !Material Constants - Thermal conductivity
          !Fibre Material
     K_lf=1.03                                 !Longitudinal thermal conductivity fibre [W/(m degC)] (Struzziero2019a)
     K_tf=1.03                                 !Transverse thermal conductivity fibre [W/(m degC)] (Struzziero2019a)

          !Resin Material
     a_kr=0.0008
     b_kr=-0.0011
     c_kr=-0.0002
     d_kr=-0.0937
     e_kr=0.22
     f_kr=0.12

          !Calculation orthotropic conductivity development
     K_r=a_kr*TEMP*DOC**2 + b_kr*TEMP*DOC + c_kr*TEMP + d_kr*DOC**2 +
    &    e_kr*DOC + f_kr
     K11=v_f*K_lf + (1-v_f)*K_r
```

```
      K22=v_f*K_r*(K_tf/K_r - 1) + K_r*(ONE/TWO - K_tf/(TWO*K_r))
     &          + K_r*(K_tf/K_r - ONE)*
     & sqrt(v_f**2-v_f+((K_tf/K_r + ONE)**2)/((TWO*K_tf/K_r - TWO)**2))
      K33=K22

            !Set orthotropic conductivity in array formation
      K(1)=K11
      K(2)=K22
      K(3)=K33

            !Material Constants - Specific heat
            !Fibre Material
      A_fcp=0.0014D3
      B_fcp=0.841D3

            !Resin Material
      A_rcp=4.6
      B_rcp=1500
      delta_rcp=-350
      C_rcp=0.28
      sigma=12.5
      rho_f=2580.0
      rho_r=1105.0

            !Calculation specific heat development
      w_f= (v_f*rho_f)/(v_f*rho_f + (1-v_f)*rho_r)
      Cp_f=A_fcp*TEMP + B_fcp
      Cp_r=A_rcp*TEMP + B_rcp +
     &     (delta_rcp/(ONE+exp(C_rcp*(TEMP-Tg-sigma))))
      Cp_c=w_f*Cp_f + (1-w_f)*Cp_r

      DUDT = Cp_c
      DU = DUDT * DTEMP
      U = U + DU - Q

      DO i=1, NTGRD
       FLUX(i) = -K(i)*DTEMDX(i)
      END DO

      DO i=1, NTGRD
       DFDG(i,i)=-K(i)
      END DO

      RETURN
      END
```